

Integrated Near Field Sensing and Communications Using Unitary Approximate Message Passing Based Matrix Factorization

Zhengdao Yuan, Qinghua Guo, *Senior Member, IEEE*, Yonina C. Eldar, *Fellow, IEEE*, and Yonghui Li, *Fellow, IEEE*

Abstract—Due to the utilization of large antenna arrays at base stations (BSs) and the operations of wireless communications in high frequency bands, mobile terminals often find themselves in the near-field of the array aperture. In this work, we address the signal processing challenges of integrated near-field localization and communication in uplink transmission of an integrated sensing and communication (ISAC) system, where the BS performs joint near-field localization and signal detection (JNFLSD). We show that JNFLSD can be formulated as a matrix factorization (MF) problem with proper structures imposed on the factor matrices. Then, leveraging the variational inference (VI) and unitary approximate message passing (UAMP), we develop a low complexity Bayesian approach to MF, called UAMP-MF, to handle a generic MF problem. We then apply the UAMP-MF algorithm to solve the JNFLSD problem, where the factor matrix structures are fully exploited. Extensive simulation results are provided to demonstrate the superior performance of the proposed method.

Index Terms—Integrated sensing and communications (ISAC), near field, localization, variational inference (VI), approximate message passing (AMP), matrix factorization (MF).

I. INTRODUCTION

Equipped with a large number of antennas at base stations (BSs), massive multiple-input-multiple-output (MIMO) technology has the potential to significantly enhance spectral efficiency by orders of magnitude, recognized as one of the key technologies for future generation of wireless communications [1], [2]. The availability of abundant spectrum resources in the millimeterwave (mmWave) and Terahertz bands presents an attractive proposition for high-frequency communications [3]. Moreover, the compact dimensions of high-frequency antennas renders them highly suitable for deploying massive MIMO systems with a large number of antennas. Consequently, high-frequency massive MIMO is widely acclaimed as a key enabler for the future of wireless communications [4].

Owing to the deployment of large antenna apertures at base stations (BSs) and the utilization of high-frequency bands,

Part of this work will be presented in ICASSP 2024.

Z. Yuan is with the Artificial Intelligence Technology Engineering Research Center, Open University of Henan, Zhengzhou 450002, China. He was with the School of Electrical, Computer and Telecommunications Engineering, University of Wollongong, Wollongong, NSW 2522, Australia (e-mail: yuan_zhengdao@foxmail.com).

Q. Guo is with the School of Electrical, Computer and Telecommunications Engineering, University of Wollongong, Wollongong, NSW 2522, Australia (e-mail: qguo@uow.edu.au).

Y. C. Eldar is with the Faculty of Mathematics and Computer Science, Weizmann Institute of Science, Rehovot 7610001, Israel (e-mail: yonina.eldar@weizmann.ac.il).

Y. Li is with the School of Electrical and Information Engineering, University of Sydney, Sydney, NSW 2006, Australia (e-mail: yonghui.li@sydney.edu.au).

mobile terminals frequently find themselves within the near-field of the array aperture. This proximity to the array is due to the fact that the Rayleigh distance, which serves as the boundary between the near-field and far-field regions, is typically large [5], [6]. For instance, consider a uniform linear antenna array comprising 128 elements with half-wavelength spacing, operating at a carrier frequency of 30GHz. In this context, the Rayleigh distance is approximately 82 meters, rendering the near-field region a significant consideration in MIMO systems. When the receiver is positioned within the near-field region, it becomes imperative to accurately model the wavefront under the spherical wavefront assumption, in contrast to the planar wavefront in the far-field region [7]–[9].

Recently, there has been a significant upsurge of interest in integrated sensing and communication (ISAC) in wireless networks [8], [10]–[13]. Sensing has now emerged as an integral element of wireless networks, e.g., localization will be a service in wireless networks for many applications such as autonomous driving. In the near-field scenario, the conventional localization techniques developed based on the far-field assumption e.g., the on-grid the angle of arrival estimation method simultaneous weighted-orthogonal matching pursuit (SW-OMP) [38], and the simultaneous iterative gridless weighted orthogonal least square (SIGW-OLS) angle estimation method [15] suffer from performance loss due to model mismatch. Recently, the problem of target localization and channel estimation in near-field environment has received tremendous attention, e.g., the works in [5], [12], [16]–[18]. The Cramer-Rao bound of target localization in near-field was studied [5], and the bound subject to minimum communication rate requirement was investigated in [12]. In large-scale massive MIMO systems, subarray-wise and scatterer-wise channel estimation methods to estimate the near-field nonstationary channel were studied in [16]. By using high-order statistics and leveraging the structure of the signal covariance matrix, subspace-based algorithms [17] and high-order MUSIC algorithms [14] were proposed to estimate angles of departure and distances between sources and receivers in the near-field. Near-field channel estimation was studied in [18], and further in [9], a near-field channel estimation algorithm (NF-SOMP) was developed to handle the case that far-field and near-field paths coexist. In this work, we focus on the issue of integrated near-field sensing and communications in the case of uplink transmission without pilot signals, where the BS assumes the dual role of user localization and signal detection, by performing blind joint near-field localization and signal detection (JNFLSD).

In this paper, we show that blind JNFLSD can be formulated

as a matrix factorization (MF) problem with imposed structures on two factor matrices, i.e., factorizing a received signal matrix \mathbf{Y} to the product of two factor matrices \mathbf{A} and \mathbf{X} with the consideration of noise perturbation, where the factor matrix \mathbf{X} is sparse and the columns of matrix \mathbf{A} are subject to the structure specified by the distance-angle dependent steering vectors. To solve a generic MF problem, leveraging variational inference (VI) [20] and unitary approximate message passing (UAMP) [21], [22], we develop an efficient Bayesian approach. In choosing the variational distribution, instead of using the mean field approximation with full factorization, we only decouple \mathbf{A} and \mathbf{X} and treat them as two latent matrices to avoid performance loss, leading to the updates of two distributions on matrices \mathbf{A} and \mathbf{X} , which are difficult and expensive. By exploiting the structure of the variational messages on \mathbf{A} and \mathbf{X} and through a covariance matrix whitening process, we incorporate UAMP into VI to efficiently deal with the updates of the distributions of \mathbf{A} and \mathbf{X} . The VI-based method is implemented using message passing with UAMP as its key component, leading to an algorithm called UAMP-MF. UAMP-MF inherits the low complexity and robustness of UAMP. Enjoying the flexibility of a Bayesian approach and low complexity and robustness of UAMP, UAMP-MF can handle various MF problems in a unified way while with high computational efficiency. We then apply the developed UAMP-MF algorithm to solve the JNFLSD problem, where the structures of the factor matrices are fully exploited. Extensive simulation results are provided to demonstrate the superior performance of the proposed method.

The remainder of this paper is organized as follows. In Section II, we introduce the signal model for integrated near-field localization and communications, and formulate JNFLSD as a matrix factorization problem. In Section III, we develop the matrix factorization algorithm UAMP-MF, leveraging VI and UAMP. In Section IV, the UAMP-MF algorithm is applied to tackle the JNFLSD problem. Simulation results are provided to demonstrate the superiority of the UAMP-MF based algorithm in Section V, and conclusions are drawn in Section VI.

Throughout the paper, we use the following notations. Bold-face lower-case and upper-case letters denote vectors and matrices, respectively. A Gaussian distribution of x with mean \hat{x} and variance ν_x is represented by $\mathcal{N}(x; \hat{x}, \nu_x)$. Notation $\text{Tr}(\cdot)$ denotes the trace operation. The relation $f(x) = cg(x)$ for some positive constant c is written as $f(x) \propto g(x)$, and $\text{diag}(\mathbf{a})$ returns a diagonal matrix with \mathbf{a} on its diagonal. We use $\mathbf{A} \cdot \mathbf{B}$ and $\mathbf{A} \cdot / \mathbf{B}$ to denote the element-wise product and division between \mathbf{A} and \mathbf{B} , respectively. The notation $|\mathbf{A}|^2$ denotes element-wise magnitude squared operation for \mathbf{A} , and $\|\mathbf{A}\|$ is the Frobenius norm of \mathbf{A} . We use $\mathbf{1}$, $\mathbf{0}$ and \mathbf{I} to denote an all-one matrix, an all-zero matrix and an identity matrix with a proper size, respectively. The above operations defined for matrices are applied to vectors. We use $\text{Vec}(\cdot)$ to denote the vectorization operation. We use $\mathcal{MN}(\mathbf{X}; \hat{\mathbf{X}}, \mathbf{U}_X, \mathbf{V}_X)$ to denote the matrix Gaussian distribution, which is a generalization of the multivariate Gaussian distribution to matrix-valued random variables [23], where \mathbf{X} is a random Gaussian matrix, $\hat{\mathbf{X}}$ is the mean of \mathbf{X} , \mathbf{U}_X and \mathbf{V}_X are the covariance among rows and columns of \mathbf{X} , respectively. The matrix Gaussian distribution is related to the multivariate Gaussian distribution in the way that $\mathbf{x} \sim \mathcal{N}(\mathbf{x}; \hat{\mathbf{x}}, \mathbf{V}_X \otimes \mathbf{U}_X)$, where $\mathbf{x} = \text{Vec}(\mathbf{X})$ and $\hat{\mathbf{x}} = \text{Vec}(\hat{\mathbf{X}})$.

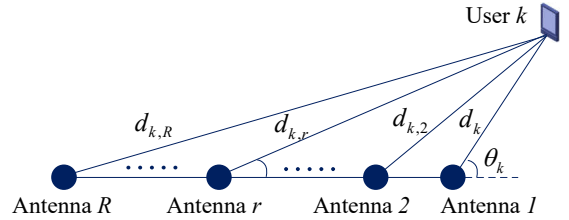


Fig. 1: Illustration of near-field angle-distance dependent signal model (only a single user is shown).

II. SIGNAL MODEL AND PROBLEM FORMULATION FOR INTEGRATED NEAR FIELD SENSING AND COMMUNICATIONS

We consider an uplink near-field ISAC system, where a BS equipped with R antennas provides communications and localization services to K single antenna users. In particular, we focus on uplink transmission, where users transmit signals to the BS, and the BS performs JNFLSD based on the received signals. It is worth highlighting that the method developed in this paper is automatically applicable to the far-field scenario because the near-field signal model degenerates to the far-field one when the distance from the BS to users is large. In addition, we assume that differentiation modulation is employed by all users, enabling that JNFLSD is realized without using pilot signals. This is significant as the training period can be skipped and considerable pilot overhead can be saved, thereby making the system attractive for the scenario of moving mobile terminals.

As shown in Fig. 1, for simplicity, we assume that a uniform linear array is used by the BS. However, we note that the method proposed in this paper can be readily extended to other array configurations. We assume that the antenna spacing is $\lambda/2$, resulting in an aperture of $D = (R - 1)\lambda/2$, where λ is the signal wavelength. The boundary between near-field and far-field is determined by the Rayleigh distance $2D^2/\lambda$ [6]. Because of the use of antenna arrays with large aperture at the BS and the short wavelength of mmWave/Terahertz band signals, there is a high probability that the users locate in the near-field of the BS. Due to the high attenuation of mmWave/Terahertz band signals, we only consider the line of sight (LOS) path between a user and the BS [24]. The distance between the k th user and the first antenna (reference point) of the antenna array at the BS is denoted by d_k , and θ_k represents the angle between the antenna array and the k th user, as shown in Fig. 1. The received signal at the r th antenna element from the k th user at time instant l can be expressed as

$$y_{r,l} = \exp\left(\frac{-j2\pi}{\lambda}(d_{k,r} - d_k)\right) x_{k,l} + w_{r,l} \quad (1)$$

where $d_{k,r}$ denotes the distance between the k th user to the r th antenna at the BS, $x_{k,l} = g_k s_{k,l}$ with g_k being the channel gain of user k (which is a constant over a short time period) and $s_{k,l}$ being the transmitted signal of user k , and $w_{r,l}$ denotes the noise. According to Fig. 1,

$$d_{k,r} - d_k = \sqrt{d_k^2 + b_r^2 + 2d_k b_r \cos \theta_k} - d_k \quad (2)$$

with $b_r = (r - 1)\lambda/2$, which is related to the angle θ_k . Hence

we define

$$\begin{aligned} a_r(d_k, \theta_k) &= \exp\left(\frac{-j2\pi}{\lambda}(d_{k,r} - d_k)\right) \\ &= \exp\left(\frac{-j2\pi}{\lambda}\left[\sqrt{d_k^2 + b_r^2 + 2d_k b_r \cos \theta_k} - d_k\right]\right) \end{aligned} \quad (3)$$

Then, for all the antenna elements, the angle-distance dependent steering vector can be represented as

$$\mathbf{a}(d_k, \theta_k) = [a_1(d_k, \theta_k), \dots, a_R(d_k, \theta_k)]^T. \quad (4)$$

Consider K users in the system, and the received signal by the BS for all users in a time duration of L sampling time instants can be expressed as

$$\mathbf{Y} = \mathbf{A}\mathbf{X} + \mathbf{W}, \quad (5)$$

where $\mathbf{X} = [\mathbf{x}_1, \dots, \mathbf{x}_K]^T \in \mathbb{C}^{K \times L}$, $\mathbf{W} \in \mathbb{C}^{R \times L}$ is the white Gaussian noise matrix, and

$$\mathbf{A} = [\mathbf{a}(d_1, \theta_1), \dots, \mathbf{a}(d_K, \theta_K)] \in \mathbb{C}^{R \times K}. \quad (6)$$

The aim of the BS is to locate the users by estimating the parameters $\{d_k, \theta_k\}$ and detect the transmitted symbols of all users based on the estimates of $\{x_{k,l}\}$. As no pilot signals are used, only the received signal matrix \mathbf{Y} is available at the BS. We have the following remarks:

- We need to factorize the received signal matrix \mathbf{Y} to the product of matrices \mathbf{A} and \mathbf{X} , plus noise matrix \mathbf{W} , thereby the estimates of the matrices $\hat{\mathbf{A}}$ and $\hat{\mathbf{X}}$ can be obtained. This is an MF problem.
- It is noted that the columns of matrix \mathbf{A} are parameterized by parameters $\{d_k, \theta_k\}$, the estimation of matrix \mathbf{A} produces the parameter estimates. As differential modulation is employed, the transmitted symbols of the users can be detected based on the estimate $\hat{\mathbf{X}}$.
- A conventional way to solve the problem is transforming the problem to a sparse signal recovery one by constructing a dictionary matrix \mathbf{A}' with a two-dimensional grid over $\{d_k, \theta_k\}$, leading to a sparse matrix \mathbf{X}' with model $\mathbf{Y} = \mathbf{A}'\mathbf{X}' + \mathbf{W}$. With the known dictionary matrix \mathbf{A}' , one only needs to recovery the sparse matrix \mathbf{X}' . However, this way is normally impractical for the considered problem because the size of the dictionary matrix is huge as the grid is established over two parameters d_k and θ_k , resulting in prohibitively high complexity. In addition, the true $\{d_k, \theta_k\}$ may not land on the grids, rendering grid mismatch errors. Off-grid methods may be used to deal with the grid-mismatch problem, but they still require the assist of a grid, which is huge for the considered problem. So the complexity is a serious concern.

In this paper, we address the problem from the perspective of MF, where the matrices \mathbf{A} and \mathbf{X} are estimated simultaneously. We start from the development of a highly efficient algorithm UAMP-MF to solve a generic MF problem, and then apply it to tackle the blind JNFLSD problem.

III. MATRIX FACTORIZATION USING UNITARY APPROXIMATE MESSAGE PASSING

We consider a generic MF problem with model (5), and abuse the use of the notation \mathbf{A} and \mathbf{X} for more general scenarios, i.e., depending on concrete application scenarios, the

matrices \mathbf{A} and \mathbf{X} are subject to some structures. For instance, in dictionary learning (DL) [25], matrix \mathbf{X} is sparse matrix and \mathbf{A} is a dictionary matrix to be learned. In compressive sensing with matrix uncertainty (CSMU) [26], \mathbf{X} is sparse and the sensing matrix \mathbf{A} can be modeled as $\mathbf{A} = \bar{\mathbf{A}} + \delta\mathbf{A}$, where the matrix $\bar{\mathbf{A}}$ is known, and $\delta\mathbf{A}$ denotes an unknown perturbation matrix. The robust principal component analysis (RPCA) problem [27] can also be formulated as (5), where both \mathbf{A} and \mathbf{X} admit specific structures [28]. We may also be interested in sparse MF, where both \mathbf{A} and \mathbf{X} are sparse. In this section, we first give a brief introduction to the VI and (U)AMP, then develop the UAMP-MF algorithm for a generic MF problem by incorporating UAMP to VI. The use of the UAMP-MF algorithm to solve the formulated JNFLSD problem will be elaborated in Section IV.

A. Variational Inference

VI is a machine learning method widely used to approximate posterior densities for Bayesian models [29], [20], [30]. Let \mathbf{V} and \mathbf{R} be the set of hidden (latent) variables and visible (observed) variables, respectively, with joint distribution $p(\mathbf{V}, \mathbf{R})$. The goal of VI is to find a tractable variational distribution $q(\mathbf{V})$ that approximates the true posterior distribution $p(\mathbf{V}|\mathbf{R})$. With the distribution $q(\mathbf{V})$, the log marginal distribution of the observed variables admits the following decomposition

$$\ln p(\mathbf{R}) = \mathcal{L}(q(\mathbf{V})) + \mathcal{KL}(q(\mathbf{V})||p(\mathbf{V}|\mathbf{R})), \quad (7)$$

where the variational lower bound $\mathcal{L}(q(\mathbf{V}))$ is given as

$$\mathcal{L}(q(\mathbf{V})) = \int_{\mathbf{V}} q(\mathbf{V}) \ln \frac{p(\mathbf{V}, \mathbf{R})}{q(\mathbf{V})}, \quad (8)$$

and the Kullback-Leibler (KL) divergence between $q(\mathbf{V})$ and $p(\mathbf{V}|\mathbf{R})$ is

$$\mathcal{KL}(q(\mathbf{V})||p(\mathbf{V}|\mathbf{R})) = - \int_{\mathbf{V}} q(\mathbf{V}) \log \frac{p(\mathbf{V}|\mathbf{R})}{q(\mathbf{V})}. \quad (9)$$

The distribution $q(\mathbf{V})$ that minimizes the KL divergence $\mathcal{KL}(q(\mathbf{V})||p(\mathbf{V}|\mathbf{R}))$ can be found by maximizing the variational lower bound $\mathcal{L}(q(\mathbf{V}))$.

VI can be implemented using message passing with the assistance of graphical models [20], [30]. If the variational distribution with some factorization is chosen, e.g.,

$$q(\mathbf{V}) = \prod_k q_k(\mathbf{V}_k), \quad (10)$$

where $\mathbf{V} = \{\mathbf{V}_k\}$, then the variational distribution can be found through an iterative procedure [20] with the update rule

$$q_k(\mathbf{V}_k) \propto \exp\left(\int_{\tilde{\mathbf{V}}} q(\tilde{\mathbf{V}}) \log f(\mathbf{V}_k, \tilde{\mathbf{V}})\right). \quad (11)$$

Here $f(\mathbf{V}_k, \tilde{\mathbf{V}})$ is a local factor associated with \mathbf{V}_k and $\tilde{\mathbf{V}} \in \{\mathbf{V}_i, i \neq k\}$, depending on the structure of the factor graph. The updates of $\{q_k(\mathbf{V}_k)\}$ are carried out iteratively until it converges or a pre-set number of iterations is reached.

B. (U)AMP

AMP was derived based on loopy BP with Gaussian and Taylor-series approximations [31], [32], which can be used to recover \mathbf{x} from the noisy measurement $\mathbf{y} = \mathbf{A}\mathbf{x} + \mathbf{w}$ with \mathbf{w} being a zero-mean white Gaussian noise vector. It works well for an i.i.d. (sub)Gaussian \mathbf{A} , but can easily diverge for generic \mathbf{A} [33]. It is shown in [21] that the robustness of AMP can be significantly improved through simple pre-processing, i.e., performing a unitary transformation to the original linear model [22]. With an SVD $\mathbf{A} = \mathbf{U}\mathbf{\Lambda}\mathbf{V}$, performing a unitary transformation with \mathbf{U}^H leads to the following model

$$\mathbf{r} = \mathbf{\Phi}\mathbf{x} + \boldsymbol{\omega}, \quad (12)$$

where $\mathbf{r} = \mathbf{U}^H\mathbf{y}$, $\mathbf{\Phi} = \mathbf{U}^H\mathbf{A} = \mathbf{\Lambda}\mathbf{V}$, $\mathbf{\Lambda}$ is rectangular diagonal matrix, and $\boldsymbol{\omega} = \mathbf{U}^H\mathbf{w}$ remains white and Gaussian.

Applying the vector step size AMP [32] with model (12) leads to the first version of UAMP (called UAMPv1) shown in Algorithm 1¹. An average operation can be applied to two vectors: $\boldsymbol{\tau}_x$ in Line 7 and $|\mathbf{\Phi}^H|^2\boldsymbol{\tau}_s$ in Line 5 of UAMPv1 in Algorithm 1, leading to the second version of UAMP [21] (called UAMPv2), where the operations in the brackets of Lines 1, 5 and 7 are executed (refer to [22] for details).

Algorithm 1 UAMP (UAMPv2 executes operations in []) ---

Initialize $\boldsymbol{\tau}_x^{(0)}$ (or $\tau_x^{(0)} > 0$) and $\mathbf{x}^{(0)}$. Set $\mathbf{s}^{(-1)} = \mathbf{0}$ and $t = 0$. Define vector $\boldsymbol{\lambda} = \mathbf{\Lambda}\mathbf{\Lambda}^H\mathbf{1}$.

Repeat

- 1: $\boldsymbol{\tau}_p = |\mathbf{\Phi}|^2\boldsymbol{\tau}_x^t$ [or $\boldsymbol{\tau}_p = \boldsymbol{\tau}_x^t\boldsymbol{\lambda}$]
- 2: $\mathbf{p} = \mathbf{\Phi}\mathbf{x}^t - \boldsymbol{\tau}_p \cdot \mathbf{s}^{t-1}$
- 3: $\boldsymbol{\tau}_s = \mathbf{1} / (\boldsymbol{\tau}_p + \beta^{-1}\mathbf{1})$
- 4: $\mathbf{s}^t = \boldsymbol{\tau}_s \cdot (\mathbf{r} - \mathbf{p})$
- 5: $\mathbf{1} / \boldsymbol{\tau}_q = |\mathbf{\Phi}^H|^2\boldsymbol{\tau}_s$ [or $\mathbf{1} / \boldsymbol{\tau}_q = (\frac{1}{N}\boldsymbol{\lambda}^H\boldsymbol{\tau}_s)\mathbf{1}$]
- 6: $\mathbf{q} = \mathbf{x}^t + \boldsymbol{\tau}_q \cdot (\mathbf{\Phi}^H\mathbf{s}^t)$
- 7: $\boldsymbol{\tau}_x^{t+1} = \boldsymbol{\tau}_q \cdot g'_x(\mathbf{q}, \boldsymbol{\tau}_q)$ [or $\tau_x^{t+1} = \frac{1}{N}\mathbf{1}^H(\boldsymbol{\tau}_q \cdot g'_x(\mathbf{q}, \boldsymbol{\tau}_q))$]
- 8: $\mathbf{x}^{t+1} = g_x(\mathbf{q}, \boldsymbol{\tau}_q)$
- 9: $t = t + 1$

Until terminated ---

In the (U)AMP algorithm, $g_x(\mathbf{q}, \boldsymbol{\tau}_q)$ is related to the prior of \mathbf{x} , which is a column vector with the n th entry given by

$$[g_x(\mathbf{q}, \boldsymbol{\tau}_q)]_n = \frac{\int x_n p(x_n) \mathcal{N}(x_n; q_n, \tau_{q_n}) dx_n}{\int p(x_n) \mathcal{N}(x_n; q_n, \tau_{q_n}) dx_n}, \quad (13)$$

where $p(x_n)$ represents a prior for x_n , and q_n and τ_{q_n} are the n th entry of \mathbf{q} and $\boldsymbol{\tau}_q$, respectively. The function $g'_x(\mathbf{q}, \boldsymbol{\tau}_q)$ returns a column vector and the n th element is denoted by $[g'_x(\mathbf{q}, \boldsymbol{\tau}_q)]_n$, where the derivative is taken with respect to q_n .

C. Design of UAMP-MF

With the Bayesian treatment of MF by transforming the constraints on matrices \mathbf{A} and \mathbf{X} to their priors $p(\mathbf{A})$ and $p(\mathbf{X})$ properly, many MF problems can be handled in a unified way. In this work, we assume that the priors are separable, i.e., $p(\mathbf{A}) = \prod_{m,n} p(h_{m,n})$ and $p(\mathbf{X}) = \prod_{n,l} p(x_{n,l})$, which can be used for NMF, DL, CSMU, RPCA and sparse MF, as shown in Section IV.

¹Replacing \mathbf{r} and $\mathbf{\Phi}$ with \mathbf{y} and \mathbf{A} , the original AMP algorithm is recovered.

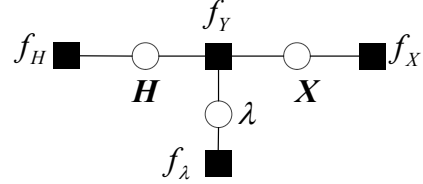


Fig. 2: Factor graph of (14), where $f_A \triangleq p(\mathbf{A})$, $f_Y \triangleq p(\mathbf{Y}|\mathbf{X}, \mathbf{A}, \lambda)$, $f_X \triangleq p(\mathbf{X})$, and $f_\lambda \triangleq p(\lambda)$.

With model (5), we have the following joint conditional distribution and its factorization

$$p(\mathbf{X}, \mathbf{A}, \lambda|\mathbf{Y}) \propto p(\mathbf{Y}|\mathbf{X}, \mathbf{A}, \lambda)p(\mathbf{X})p(\mathbf{A})p(\lambda), \quad (14)$$

where we assume that the entries of \mathbf{W} are i.i.d. Gaussian with zero mean precision λ (this is applied to all the examples in this paper), and

$$p(\mathbf{Y}|\mathbf{X}, \mathbf{A}, \lambda) = \mathcal{MN}(\mathbf{Y}; \mathbf{A}\mathbf{X}, \mathbf{I}_M, \lambda^{-1}\mathbf{I}_L). \quad (15)$$

We assume a Jefferys prior $p(\lambda) \propto 1/\lambda$ [34] for the noise precision.

If the a posteriori distributions $p(\mathbf{A}|\mathbf{Y})$ and $p(\mathbf{X}|\mathbf{Y})$ can be found, then the estimates of \mathbf{A} and \mathbf{X} can be obtained, e.g., using the a posteriori means of \mathbf{A} and \mathbf{X} to serve as their estimates. However, it is intractable to find the exact a posteriori distributions in general, so we resort to VI to find their variational approximations. We define a variational distribution

$$q(\mathbf{X}, \mathbf{A}, \lambda) = q(\mathbf{X})q(\mathbf{A})q(\lambda), \quad (16)$$

and expect that $q(\mathbf{X}) \approx p(\mathbf{X}|\mathbf{Y})$, $q(\mathbf{A}) \approx p(\mathbf{A}|\mathbf{Y})$ and $q(\lambda) \approx p(\lambda|\mathbf{Y})$. However, finding the variational distributions is still challenging due to the high dimensions of \mathbf{A} and \mathbf{X} , and the priors of \mathbf{A} and \mathbf{X} may also lead to intractable $q(\mathbf{A})$ and $q(\mathbf{X})$. In this work, UAMP is employed to solve these challenges with high efficiency. This also leads to Gaussian approximations to $q(\mathbf{A})$ and $q(\mathbf{X})$, so that the estimates of \mathbf{A} and \mathbf{X} (i.e., the a posteriori means of \mathbf{A} and \mathbf{X}) appear as the parameters of the distributions. Leveraging UAMP, we carry out VI in a message passing manner, with the aid of a factor graph representation of the problem, depicted in Fig.2. This leads to the message passing algorithm UAMP-MF.

Next, we derive the UAMP-MF algorithm and show how to efficiently update $q(\mathbf{X})$, $q(\mathbf{A})$ and $q(\lambda)$ iteratively. In the derivation of UAMP-MF, we use the notation $m_{n_a \rightarrow n_b}(\mathbf{X})$ to denote a message passed from node n_a to node n_b , which is a function of \mathbf{X} . The UAMP-MF algorithm is shown in Algorithm 2, which we will frequently refer to in this section.

1) *Update of $q(\mathbf{X})$* : According to VI, with $q(\mathbf{A})$ and $q(\lambda)$ (updated in the last iteration), we compute $q(\mathbf{X})$. As shown by the factor graph in Fig. 2, we need to compute the message $m_{f_Y \rightarrow X}(\mathbf{X})$ from the factor node f_Y to the variable node \mathbf{X} and then combine it with the prior $p(\mathbf{X})$. Later we will see that $q(\mathbf{A})$ is a matrix Gaussian distribution, i.e., $q(\mathbf{A}) = \mathcal{MN}(\mathbf{A}; \hat{\mathbf{A}}, \mathbf{U}_A, \mathbf{V}_A)$ with a mean matrix $\hat{\mathbf{A}}$ (see Line 23 of Algorithm 2), a column covariance matrix \mathbf{V}_A and row covariance matrix $\mathbf{U}_A = \mathbf{I}_N$, and $q(\lambda)$ is a Gamma distribution. It turns out that $m_{f_Y \rightarrow X}(\mathbf{X})$ is matrix Gaussian, shown by Proposition 1.

Algorithm 2 UAMP-MF

Initialization: $U_A = I$, $V_A = I$, $\hat{A} = \mathbf{1}$, $V_X = I$. $\Xi_X = \mathbf{1}$, $S_X = \mathbf{0}$, $\Xi_A = \mathbf{1}$, and $S_A = \mathbf{0}$.

Repeat

- 1: $\overline{W}_X = \hat{A}^H \hat{A} + M V_A$
- 2: $[C_X, D_X] = \text{eig}(\overline{W}_X)$
- 3: $R_X = D_X^{-\frac{1}{2}} C_X^H \hat{A}^H Y$, $\Phi_X = D_X^{-\frac{1}{2}} C_X^H$
- 4: $V_{P_X} = |\Phi_X|^2 \Xi_X$
- 5: $P_X = \Phi_X \hat{X} - V_{P_X} \cdot S_X$
- 6: $V_{S_X} = \mathbf{1} / (V_{P_X} + \lambda^{-1} \mathbf{1})$
- 7: $S_X = V_{S_X} \cdot (R_X - P_X)$
- 8: $V_{Q_X} = \mathbf{1} / (|\Phi_X|^2 V_{S_X})$
- 9: $Q_X = \hat{X} + V_{Q_X} \cdot (\Phi_X^H S_X)$
- 10: $\Xi_X = V_{Q_X} \cdot G'_X(Q_X, V_{Q_X})$
- 11: $\hat{X} = G_X(Q_X, V_{Q_X})$
- 12: $U_X = \text{diag}(\text{mean}(\Xi_X, 2))$
- 13: $\overline{W}_A = \hat{X} \hat{X}^H + L U_X$
- 14: $[C_A, D_A] = \text{eig}(\overline{W}_A)$
- 15: $R_A = D_A^{-\frac{1}{2}} C_A^H \hat{X} Y^H$, $\Phi_A = D_A^{-\frac{1}{2}} C_A^H$
- 16: $V_{P_A} = |\Phi_A|^2 \Xi_A$
- 17: $P_A = \Phi_A \hat{A} - V_{P_A} \cdot S_A$
- 18: $V_{S_A} = \mathbf{1} / (V_{P_A} + \lambda^{-1} \mathbf{1})$
- 19: $S_A = V_{S_A} \cdot (R_A - P_A)$
- 20: $V_{Q_A} = \mathbf{1} / (|\Phi_A|^2 V_{S_A})$
- 21: $Q_A = \hat{A} + V_{Q_A} \cdot (\Phi_A^H S_A)$
- 22: $\Xi_A = V_{Q_A} \cdot G'_A(Q_A, V_{Q_A}^T)$
- 23: $\hat{A} = G_A(Q_A, V_{Q_A}^T)$
- 24: $V_A = \text{diag}(\text{mean}(\Xi_A, 1))$
- 25: $\hat{\lambda} = ML/C$ with C given in

Until terminated

Proposition 1: The message from f_Y to \mathbf{X} can be expressed as a matrix Gaussian distribution, i.e.,

$$m_{f_Y \rightarrow X}(\mathbf{X}) \propto \mathcal{MN}(\mathbf{X}; \overline{\mathbf{X}}, \hat{\lambda}^{-1} \overline{U}_X, \mathbf{I}_L), \quad (17)$$

with

$$\overline{\mathbf{X}} = \overline{U}_X \hat{A}^H Y, \quad (18)$$

$$\overline{U}_X = (\hat{A}^H \hat{A} + \text{Tr}(U_A) V_A)^{-1}, \quad (19)$$

and

$$\hat{\lambda} = \int_{\lambda} \lambda q(\lambda). \quad (20)$$

The computation of $\hat{\lambda}$ is shown in (46).

Proof. See Appendix A. \square

Then the message $m_{f_Y \rightarrow X}(\mathbf{X})$ needs to be combined with the prior $p(\mathbf{X})$ to obtain $q(\mathbf{X})$. This can be challenging as \mathbf{X} is a random matrix with high dimension, and the prior $p(\mathbf{X})$ may lead to an intractable $q(\mathbf{X})$ and high computational complexity. Next, leveraging UAMP, we update $q(\mathbf{X})$ efficiently. In addition, we will also circumvent the matrix inversion involved in (19).

Note that $\mathbf{X} = [x_1, \dots, x_l]$ and $\overline{\mathbf{X}} = [\overline{x}_1, \dots, \overline{x}_l]$. The result in (17) indicates that $x_l \sim \mathcal{N}(x_l; \overline{x}_l, \hat{\lambda}^{-1} \overline{U}_X)$, and all vectors in \mathbf{X} have a common covariance matrix, which will greatly

simplify the computations later. With the result, for each x_l , we have the following pseudo observation model

$$\overline{x}_l = x_l + e_l, \quad (21)$$

where $e_l \sim \mathcal{N}(e_l; 0, \hat{\lambda}^{-1} \overline{U}_X)$, i.e., the model noise is not white. We can whiten the noise by left-multiplying both sides of (21) by $\overline{U}_X^{-\frac{1}{2}}$, leading to

$$\overline{U}_X^{-\frac{1}{2}} \overline{x}_l = \overline{U}_X^{-\frac{1}{2}} x_l + w_l, \quad (22)$$

where $w_l = \overline{U}_X^{-\frac{1}{2}} e_l$ is white and Gaussian with covariance $\hat{\lambda}^{-1} I$. Through the whitening operation, we get a standard linear model with white additive Gaussian noise, which facilitates the use of UAMP. Considering all the vectors in $\overline{\mathbf{X}}$ which share the same whitening matrix, we have

$$\overline{U}_X^{-\frac{1}{2}} \overline{\mathbf{X}} = \overline{U}_X^{-\frac{1}{2}} \mathbf{X} + \Omega_X, \quad (23)$$

where Ω_X is white and Gaussian.

With model (23) and the prior $p(\mathbf{X})$, we use UAMP to update $q(\mathbf{X})$. Following UAMP, a unitary transformation needs to be performed with the unitary matrix C_X^H obtained from the SVD of $\overline{U}_X^{-\frac{1}{2}}$ (or eigenvalue decomposition (EVD) as the matrix is definite and symmetric), i.e.,

$$\overline{U}_X^{-\frac{1}{2}} = C_X \Lambda C_X^H \quad (24)$$

with Λ being a diagonal matrix. After performing the unitary transformation, we have

$$R_X = \Phi_X \mathbf{X} + \Omega'_X, \quad (25)$$

where $R_X = C_X^H \overline{U}_X^{-\frac{1}{2}} \overline{\mathbf{X}}$, $\Phi_X = C_X^H \overline{U}_X^{-\frac{1}{2}} = \Lambda C_X^H$ and $\Omega'_X = C_X^H \Omega_X$, which is still Gaussian and white.

From the above, the direct way to obtain R_X and Φ_X in model (25) are costly. Specifically, a matrix inverse operation needs to be performed according to (19) so that $\overline{\mathbf{X}}$ in (18) can be obtained; a matrix squared root operation is needed to obtain $\overline{U}_X^{-\frac{1}{2}}$; and an SVD operation is required to C_X^H , which lead to high complexity. Next, we show that these expensive computations can be avoided with an EVD operation.

Instead of computing \overline{U}_X^{-1} and $\overline{U}_X^{-\frac{1}{2}}$ followed by SVD of $\overline{U}_X^{-\frac{1}{2}}$, we perform EVD to $\overline{U}_X^{-1} = \overline{W}_X^{-1} = \hat{A}^H \hat{A} + \text{Tr}(U_A) V_A$, i.e.,

$$[C_X, D_X] = \text{eig}(\overline{W}_X), \quad (26)$$

where the diagonal matrix

$$D_X = \Lambda^{-2}. \quad (27)$$

Hence $\Phi_X = \Lambda C_X^H = D_X^{-1/2} C_X^H$, where the computation of $D_X^{-1/2}$ is trivial as D_X is a diagonal matrix. Meanwhile, the computation of the pseudo observation matrix R_X can also be simplified:

$$\begin{aligned} R_X &= C_X^H \overline{U}_X^{-\frac{1}{2}} \overline{\mathbf{X}} \\ &= C_X^H \overline{U}_X^{-\frac{1}{2}} \overline{U}_X \hat{A}^H Y \\ &= D_X^{-\frac{1}{2}} C_X^H \hat{A}^H Y. \end{aligned} \quad (28)$$

For convenience, we rewrite the unitary transformed pseudo observation model as

$$\underbrace{D_X^{-\frac{1}{2}} C_X^H \hat{A}^H Y}_{R_X} = \underbrace{D_X^{-\frac{1}{2}} C_X^H}_{\Phi_X} \mathbf{X} + \Omega'_X. \quad (29)$$

The above leads to Lines 1-3 of UAMP-MF in Algorithm 2.

Due to the prior $p(\mathbf{X})$, the use of exact $q(\mathbf{X})$ often makes the message update intractable. Following (U)AMP, we perform the minimum mean squared error (MMSE) estimation based on the pseudo observation model (29) with prior $p(\mathbf{X})$, i.e., project it to be Gaussian. These correspond to Lines 4-11 of UAMP-MF. Noting that the prior $p(\mathbf{X})$ is separable, i.e., $p(\mathbf{X}) = \prod_{n,l} p(x_{nl})$, the operations in Lines 10 and 11 are element-wise, i.e., the function $G_X(\mathbf{Q}_X, V_{\mathbf{Q}_X})$ is an element-wise function with each entry same as (13) (similarly, $G'_X(\mathbf{Q}_X, V_{\mathbf{Q}_X})$ denotes its derivative). This is explained as follows. Due to the decoupling of (U)AMP, we assume the following scalar pseudo models

$$q_{nl} = x_{nl} + w_{nl}, n = 1, \dots, N, l = 1, \dots, L, \quad (30)$$

where q_{nl} is the (n, l) th element of \mathbf{Q}_X in Line 9 of the UAMP-MF algorithm, w_{nl} represents a Gaussian noise with mean zero and variance v_{nl} , and v_{nl} is the (n, l) th element of $\mathbf{V}_{\mathbf{Q}_X}$ in Line 8 of the UAMP-MF algorithm. This is significant as the complex estimation is reduced to much simpler MMSE estimation based on a number of scalar models (30) with prior $p(x_{nl})$. With the notations in Lines 10 and 11, for each entry x_{nl} in \mathbf{X} , the MMSE estimation leads to a Gaussian distribution

$$\tilde{q}(x_{nl}) = \mathcal{N}(x_{nl}; \hat{x}_{nl}, v_{x_{nl}}), \quad (31)$$

where \hat{x}_{nl} and $v_{x_{nl}}$ is the (n, l) th element of $\hat{\mathbf{X}}$ in Line 11 and the (n, l) th element of Ξ_X in Line 10, respectively. We can see that each element x_{nl} has its own variance. To facilitate subsequent processing, we make an approximation by performing an average operation to each row of Ξ_X , i.e., replacing the entries of each row of Ξ_X by their average. Then $\{\tilde{q}(x_{nl})\}$ are collectively characterized by a matrix normal distribution, i.e., $q(\mathbf{X}) = \mathcal{MN}(\mathbf{X}; \hat{\mathbf{X}}, \mathbf{U}_X, \mathbf{V}_X)$ with $\mathbf{U}_X = \text{diag}(\text{mean}(\Xi_X, 2))$ and $\mathbf{V}_X = \mathbf{I}_L$, where $\text{mean}(\Xi_X, 2)$ represents the average operation on the rows of Ξ_X . This leads to Line 12 of UAMP-MF in algorithm 2.

2) *Update of $q(\mathbf{A})$* : With the updated $q(\mathbf{X}) = \mathcal{MN}(\mathbf{X}; \hat{\mathbf{X}}, \mathbf{U}_X, \mathbf{V}_X)$ and $q(\lambda)$, we compute the message from f_Y to \mathbf{A} according to VI. Regarding the message, we have the following result.

Proposition 2: The message from f_Y to \mathbf{A} can be expressed as a matrix Gaussian distribution, i.e.,

$$m_{f_Y \rightarrow H}(\mathbf{A}) \propto \mathcal{MN}(\mathbf{A}; \bar{\mathbf{A}}, \mathbf{I}_M, \hat{\lambda}^{-1} \bar{\mathbf{V}}_A), \quad (32)$$

with

$$\bar{\mathbf{A}} = \mathbf{Y} \hat{\mathbf{X}}^H \bar{\mathbf{V}}_A, \quad (33)$$

and

$$\bar{\mathbf{V}}_A = \left(\hat{\mathbf{X}} \hat{\mathbf{X}}^H + \text{Tr}(\mathbf{V}_X) \mathbf{U}_X \right)^{-1}, \quad (34)$$

where $\hat{\lambda} = \int_{\lambda} \lambda q(\lambda)$.

Proof. See Appendix B. \square

Then we combine the message $m_{f_Y \rightarrow H}(\mathbf{A})$ with the prior of \mathbf{A} to update $q(\mathbf{A})$, which can also be realized with UAMP through a whitening operation. The procedure is similar to that for $q(\mathbf{X})$, and the difference is that the pseudo model is established row by row (rather than column by column) by considering the form of message $m_{f_Y \rightarrow H}(\mathbf{A})$.

With the message $m_{f_Y \rightarrow H}(\mathbf{A})$ and noting that

$$\bar{\mathbf{A}} = [\bar{\mathbf{a}}_1, \dots, \bar{\mathbf{a}}_M]^T \quad (35)$$

where $\bar{\mathbf{a}}_m^H \in \mathcal{R}^{1 \times N}$ is the m th row vector of $\bar{\mathbf{A}}$, we have the pseudo observation model

$$\bar{\mathbf{a}}_m = \mathbf{a}_m + \mathbf{e}_m, \quad (36)$$

where $\mathbf{e}_m \sim \mathcal{N}(\mathbf{e}_m; 0, \hat{\lambda}^{-1} \bar{\mathbf{V}}_A)$. Performing whitening operation to (36) leads to

$$\bar{\mathbf{V}}_A^{-\frac{1}{2}} \bar{\mathbf{a}}_m = \bar{\mathbf{V}}_A^{-\frac{1}{2}} \mathbf{a}_m + \mathbf{w}_m, \quad (37)$$

where $\mathbf{w}_m = \bar{\mathbf{V}}_A^{-\frac{1}{2}} \mathbf{e}_m$, which is white and Gaussian with covariance $\hat{\lambda}^{-1} \mathbf{I}$. Collecting all rows and representing them in matrix form, we have

$$\bar{\mathbf{V}}_A^{-\frac{1}{2}} \bar{\mathbf{A}}^H = \bar{\mathbf{V}}_A^{-\frac{1}{2}} \mathbf{A}^H + \mathbf{\Omega}_A. \quad (38)$$

UAMP is then performed based on model (38). Using the idea for updating $q(\mathbf{X})$, we obtain the unitary transformed model efficiently. We first perform an EVD to matrix $\bar{\mathbf{V}}_A^{-1} = \bar{\mathbf{W}}_A = \hat{\mathbf{X}} \hat{\mathbf{X}}^H + \text{Tr}(\mathbf{V}_X) \mathbf{U}_X$, i.e.,

$$[\mathbf{C}_A, \mathbf{D}_A] = \text{eig}(\bar{\mathbf{W}}_A). \quad (39)$$

Then the unitary transformed model is given as

$$\mathbf{R}_A^H = \mathbf{\Phi}_A^H \mathbf{A}^H + \mathbf{\Omega}'_A \quad (40)$$

where

$$\mathbf{\Phi}_A = \mathbf{D}_A^{-\frac{1}{2}} \mathbf{C}_A^H \quad (41)$$

$$\mathbf{R}_A = \mathbf{D}_A^{-\frac{1}{2}} \mathbf{C}_A^H \hat{\mathbf{X}} \mathbf{Y}^H, \quad (42)$$

and $\mathbf{\Omega}'_A$ is Gaussian and white. The above leads to Lines 13-15 of UAMP-MF in Algorithm 2.

Following UAMP in Algorithm 1, we obtain $q(\mathbf{A})$ and project it to be Gaussian, which correspond to Lines 16-23 of UAMP-MF Algorithm 2. The function $G_A(\mathbf{Q}_A, V_{\mathbf{Q}_A})$ is an element-wise function with each entry similar to (13). In addition, similar to the case for updating $q(\mathbf{X})$, to accommodate $\{q(h_{mn})\}$ with a matrix Gaussian distribution, we make an approximation by performing an average operation to each column of Ξ_A , replacing the entries of each column in Ξ_A by their average. Then $q(\mathbf{A}) = \mathcal{MN}(\mathbf{A}; \hat{\mathbf{A}}, \mathbf{U}_A, \mathbf{V}_A)$ with $\mathbf{V}_A = \text{diag}(\text{mean}(\Xi_A, 1))$ and $\mathbf{U}_A = \mathbf{I}_M$ (i.e., Line 24 of Algorithm 2), where $\text{mean}(\Xi_A, 1)$ represents the average operation on the columns of Ξ_A .

3) *Update of $q(\lambda)$* : With $q(\mathbf{A}) = \mathcal{MN}(\mathbf{A}; \hat{\mathbf{A}}, \mathbf{V}_A, \mathbf{I}_M)$ and $q(\mathbf{X}) = \mathcal{MN}(\mathbf{X}; \hat{\mathbf{X}}, \mathbf{I}_L, \mathbf{U}_X)$, we compute the message from f_Y to λ , as shown in Proposition 3.

Proposition 3: The message from f_Y to λ can be expressed as

$$m_{f_Y \rightarrow \lambda}(\lambda) \propto \lambda^{ML} \exp(-\lambda C), \quad (43)$$

where

$$C = \|\mathbf{Y} - \hat{\mathbf{A}} \hat{\mathbf{X}}\|^2 + M \text{Tr}(\hat{\mathbf{X}} \hat{\mathbf{X}}^H \mathbf{V}_A) + L \text{Tr}(\mathbf{U}_X \hat{\mathbf{A}}^H \hat{\mathbf{A}}) + M L \text{Tr}(\mathbf{U}_X \mathbf{V}_A). \quad (44)$$

Proof. See Appendix C. \square

We then combine the message $m_{f_Y \rightarrow \lambda}(\lambda)$ and the prior $p(\lambda) \propto 1/\lambda$ to update $q(\lambda)$, i.e.,

$$q(\lambda) \propto m_{f_Y \rightarrow \lambda}(\lambda)p(\lambda) = \lambda^{ML-1} \exp(-\lambda C), \quad (45)$$

which is a Gamma distribution. Then the mean of λ is obtained as

$$\hat{\lambda} = \int_{\lambda} \lambda q(\lambda) = ML/C, \quad (46)$$

which is Line 25 of UAMP-MF.

4) *Discussion and Computational Complexity:* Regarding UAMP-MF in Algorithm 2, we have the following remarks:

- We do not specify the priors of \mathbf{A} and \mathbf{X} in Algorithm 2. The detailed implementations of Lines 10, 11, 22 and 23 of the algorithm depends on the priors in a concrete scenario.
- As the MF problem often has local minima, we can use the strategy of restart to mitigate the issue of being stuck at local minima. In addition, the iterative process can be terminated based on some criterion, e.g., the normalized difference between the estimates of two consecutive iterations is smaller than a threshold.
- There are often hyper-parameters in the priors of \mathbf{A} and \mathbf{X} . If we do not have knowledge on these hyper-parameters, their values need to be leaned or tuned automatically. Thanks to the factor graph and message passing framework, these extra tasks can be implemented by extending the factor graph in Fig. 1. Some details are provided in next subsection.
- We see that UAMP-MF in Algorithm 1 involves matrix multiplications and two EVDs per iteration, which dominate its complexity. The complexity of the algorithm is therefore in a cubic order, which is low in a MF problem (the complexity of two matrices product is cubic)
- We can also see that the space cost of the algorithm is in the same order of the size of the MF problem, which is reasonable.

D. Hyper-Parameter Learning

We take MF with a sparse factor matrix as example to show how to learn the hyper-parameters in the priors by taking advantage of the factor graph and message passing techniques. We assume that \mathbf{X} is sparse and its sparsity rate is unknown. In this case, we can employ the sparsity inducing hierarchical Gaussian-Gamma prior, which is used in SBL [34]². Hence, $p(x_{nl}|\gamma_{nl}) = \mathcal{N}(x_{nl}; 0, \gamma_{nl}^{-1})$ and $p(\gamma_{nl}) = Ga(\gamma_{nl}; \epsilon, \eta)$ with ϵ and η being the shape parameter and scale parameter. While the precision γ_{nl} is to be learned, the values for ϵ and η are often set empirically, e.g., $\epsilon = \eta = 0$ [34]. It is worth mentioning that ϵ can also be tuned automatically to improve the performance [37].

The factor graph representation for this part is shown in Fig. 2. Next, we show the message updates in this sub-graph. Due to the decoupling of UAMP as shown by the pseudo model (30), the incoming message to the factor graph in Fig. 2 is Gaussian, i.e.,

$$m_{x_{nl} \rightarrow f_{x_{nl}}}(x_{nl}) = \mathcal{N}(x_{nl}; q_{nl}, v_{nl}). \quad (47)$$

²Other sparsity inducing priors may also be used, such as the spike and slab prior [35] and horseshoe prior to achieve better robustness [36].

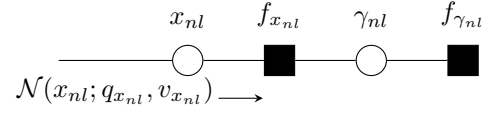


Fig. 3: Factor graph for hyper-parameters learning, where $f_{x_{nl}} \triangleq p(x_{nl}|\gamma_{nl})$ and $f_{\gamma_{nl}} \triangleq p(\gamma_{nl})$.

We perform inference on x_{nl} and γ_{nl} , which can also be achieved by using VI with a variational distribution $q(x_{nl}, \gamma_{nl}) = q(x_{nl})q(\gamma_{nl})$.

According to VI,

$$\begin{aligned} q(x_{nl}) &\propto m_{x_{nl} \rightarrow f_{x_{nl}}}(x_{nl})m_{f_{x_{nl}} \rightarrow x_{nl}}(x_{nl}) \\ &\propto \mathcal{N}(x_{nl}; \hat{x}_{nl}, v_{x_{nl}}) \end{aligned} \quad (48)$$

with $m_{f_{x_{nl}} \rightarrow x_{nl}}(x_{nl})$ shown in (52), and

$$v_{x_{nl}} = \frac{v_{q_{nl}}}{1 + \hat{\gamma}_{nl}v_{q_{nl}}}, \quad \hat{x}_{nl} = \frac{\hat{q}_{nl}}{1 + \hat{\gamma}_{nl}v_{q_{nl}}}. \quad (49)$$

The message $m_{f_{x_{nl}} \rightarrow \gamma_{nl}}(\gamma_{nl})$ can be expressed as

$$\begin{aligned} m_{f_{x_{nl}} \rightarrow \gamma_{nl}}(\gamma_{nl}) &\propto \exp\left(\int_{x_{nl}} q(x_{nl}) \log \mathcal{N}(x_{nl}; 0, \gamma_{nl}^{-1})\right), \\ &\propto \gamma_{nl} \exp(-\gamma_{nl}(|\hat{x}_{nl}|^2 + v_{x_{nl}})). \end{aligned} \quad (50)$$

The message $m_{f_{\gamma_{nl}} \rightarrow \gamma_{nl}}(\gamma_{nl}) \propto \gamma_{nl}^{\epsilon-1} \exp(-\eta\gamma_{nl})$. According to VI,

$$\begin{aligned} q(\gamma_{nl}) &\propto m_{f_{\gamma_{nl}} \rightarrow \gamma_{nl}}(\gamma_{nl})m_{f_{x_{nl}} \rightarrow \gamma_{nl}}(\gamma_{nl}) \\ &\propto \gamma_{nl}^{\epsilon} \exp(-\gamma_{nl}(|\hat{x}_{nl}|^2 + v_{x_{nl}} + \eta)). \end{aligned} \quad (51)$$

Thus

$$\begin{aligned} m_{f_{x_{nl}} \rightarrow x_{nl}}(x_{nl}) &\propto \exp\left(\int_{\gamma_{nl}} q(\gamma_{nl}) \log \mathcal{N}(x_{nl}; 0, \gamma_{nl}^{-1})\right), \\ &\propto \mathcal{N}(x_{nl}; 0, \hat{\gamma}_{nl}^{-1}), \end{aligned} \quad (52)$$

where

$$\hat{\gamma}_{nl} = \frac{1 + \epsilon}{\eta + v_{x_{nl}} + |\hat{x}_{nl}|^2}. \quad (53)$$

The above computations for all the entries of \mathbf{X} can be collectively expressed as

$$\Xi_{\mathbf{X}} = \mathbf{V}_{Q_{\mathbf{X}}} ./ \left(\mathbf{1} + \hat{\Gamma} \cdot \mathbf{V}_{Q_{\mathbf{X}}} \right), \quad (54)$$

$$\hat{\mathbf{X}} = \hat{\mathbf{Q}}_{\mathbf{X}} ./ \left(\mathbf{1} + \hat{\Gamma} \cdot \mathbf{V}_{Q_{\mathbf{X}}} \right), \quad (55)$$

$$\hat{\Gamma} = (\mathbf{1} + \epsilon \mathbf{1}) ./ \left(\eta \mathbf{1} + \Xi_{\mathbf{X}} + |\hat{\mathbf{X}}|^2 \right), \quad (56)$$

where $\hat{\Gamma}$ is a matrix with $\{\gamma_{nl}\}$ as its entries.

IV. UAMP-MF FOR INTEGRATED NEAR FIELD LOCALIZATION AND COMMUNICATIONS

In this section, we apply the developed UAMP-MF algorithm to tackle the JNFLSD problem. It is noted that the application is not straightforward as the matrix \mathbf{A} has a structure with its columns given as steering vectors parameterized by $\{d_k, \theta_k\}$.

An advantage of integrating UAMP with VI in developing the UAMP-MF algorithm is that it facilitates the reinforcement of the structure of \mathbf{A} thanks to the decoupling of UAMP, i.e.,

by executing Lines 20-21, which produce \mathbf{V}_{Q_A} and \mathbf{Q}_A , we have the following pseudo model

$$\mathbf{q}_{A,z} = \mathbf{a}(d_z, \theta_z) + \mathbf{w}_z, z = 1, \dots, Z, \quad (57)$$

where $\mathbf{q}_{A,z}$ is the z th column of \mathbf{Q}_A , and \mathbf{w}_z is approximated to a white noise with mean zero and variance $\sigma^2 = \langle \mathbf{V}_{Q_A} \rangle$. Next, we estimate d_z and θ_z based on the above model. To simplify the notations, we drop the subscript z in this section.

The challenge lies in the non-linearity of $\mathbf{a}(d, \theta)$ on the parameters d and θ . To overcome the challenge, we adopt a dynamic linearization method detailed in the following. As the algorithm is an iterative one, where the estimates of d and θ in the last round of iteration, denoted by d' and θ' , are available. Then the partial derivative vector $\mathbf{e}_\theta(d', \theta')$ and $\mathbf{e}_d(d', \theta')$ can be expressed as

$$\mathbf{e}_\theta(d', \theta') = \left. \frac{\partial \mathbf{a}(d, \theta)}{\partial \theta} \right|_{d=d', \theta=\theta'} = [e_{\theta_1}, \dots, e_{\theta_R}]^T, \quad (58)$$

$$\mathbf{e}_d(d', \theta') = \left. \frac{\partial \mathbf{a}(d, \theta)}{\partial d} \right|_{d=d', \theta=\theta'} = [e_{d_1}, \dots, e_{d_R}]^T, \quad (59)$$

where

$$\begin{aligned} e_{\theta_r} &\triangleq \left. \frac{\partial a_r(d, \theta)}{\partial \theta} \right|_{d=d', \theta=\theta'} = a_r(d', \theta') \\ &\times \left(\frac{j2\pi}{\lambda} db_r \sin \theta' \sqrt{d'^2 + b_r^2 + 2d'b_r \cos \theta'} \right) \\ e_{d_r} &\triangleq \left. \frac{\partial a_r(d, \theta)}{\partial d} \right|_{d=d', \theta=\theta'} = a_r(d', \theta') \\ &\times \frac{-j2\pi}{\lambda} \left(\sqrt{d'^2 + b_r^2 + 2d'b_r \cos \theta'} (d' + b_r \cos \theta') - 1 \right). \end{aligned} \quad (60)$$

$$(61)$$

Hence, with the first-order Taylor expansion, the vector $\mathbf{a}(d, \theta)$ can be approximately linearized at (d', θ') as

$$\begin{aligned} \mathbf{a}(d, \theta) &\approx \mathbf{a}(d', \theta') + \mathbf{e}_\theta(d', \theta')(\theta - \theta') + \mathbf{e}_d(d', \theta')(d - d') \\ &= \mathbf{a}' + \mathbf{e}'_\theta(\theta - \theta') + \mathbf{e}'_d(d - d'), \end{aligned} \quad (62)$$

where $\mathbf{a}' \triangleq \mathbf{a}(d', \theta')$, $\mathbf{e}'_\theta \triangleq \mathbf{e}_\theta(d', \theta')$ and $\mathbf{e}'_d \triangleq \mathbf{e}_d(d', \theta')$.

According to (57) and (62), we have

$$\boldsymbol{\xi}_z = \mathbf{q}_{A,z} - \mathbf{a}' = \mathbf{E}_z \mathbf{c}_z + \mathbf{w}_z, \quad (63)$$

where

$$\mathbf{E} = [\mathbf{e}_d, \mathbf{e}_\theta], \quad (64)$$

$$\mathbf{c} = \begin{bmatrix} d - d' \\ \theta - \theta' \end{bmatrix}. \quad (65)$$

Then, with model (63), we perform a LS estimation of \mathbf{c} , which is equivalent to the MMSE estimation with a priori mean $\mathbf{c}^a = 0$ and an inverse of covariance matrix $\mathbf{V}_c^a = 0$, i.e.,

$$\mathbf{V}_c = \left(\frac{1}{\sigma^2} \mathbf{E}^H \mathbf{E} \right)^{-1}, \quad (66)$$

$$\hat{\mathbf{c}} = \sigma^{-2} \mathbf{V}_c \mathbf{E}^H \boldsymbol{\xi}. \quad (67)$$

Then we can get the updated estimates of d and θ as

$$\begin{bmatrix} \hat{d} \\ \hat{\theta} \end{bmatrix} = \hat{\mathbf{c}} + \begin{bmatrix} d' \\ \theta' \end{bmatrix}. \quad (68)$$

For the LS estimation, we have the following remarks:

- As the LS estimation is a special case of the MMSE estimation, the matrix computed in (66) is actually the a posteriori

covariance matrix of \mathbf{A} , which facilitates the incorporation of the estimation to the UAMP-MF algorithm.

- The computational complexity involved in (66) and (67) is low due to the small size of the matrices, i.e., $\mathbf{E}^H \mathbf{E}$ and \mathbf{V}_c are 2×2 matrices.

In the above, we only detail the computations for a single column of \mathbf{Q}_A . After applying it to all the columns, we can get $\{\hat{d}_z, \hat{\theta}_z\}$. Then according to the UAMP-MF algorithm, we need to produce the estimate $\hat{\mathbf{A}}$ and the covariance matrix $\boldsymbol{\Xi}_A$. With the estimates $\{\hat{d}_z, \hat{\theta}_z\}$, it is straightforward to obtain that

$$\hat{\mathbf{A}} = [\mathbf{a}(d_1, \theta_1), \dots, \mathbf{a}(d_Z, \theta_Z)]. \quad (69)$$

For the computation of the covariance matrix, we use the linearized model (62) for each column of \mathbf{A} and then average them, leading to

$$\boldsymbol{\Xi}_A = \frac{1}{Z} \sum_z \mathbf{E}_z \mathbf{V}_{c_z} \mathbf{E}_z^H. \quad (70)$$

Algorithm 3 UAMP-MF Based JNFLSD Algorithm

Initialization: $\tilde{K} = U_{max}$, $\mathbf{U}_A = \mathbf{I}_R$, $\hat{\mathbf{A}} = \mathbf{A}^0$, $\mathbf{V}_X = \mathbf{I}_L$.

Repeat

- 1: Execute Lines (1)-(10) of UAMP-MF in Algorithm 2 to obtain \mathbf{Q}_X and \mathbf{V}_{Q_X}
- 2: $\hat{\mathbf{X}} = \mathbf{Q}_X \cdot / (1 + \mathbf{V}_{Q_X} \cdot \boldsymbol{\Gamma})$
- 3: $\boldsymbol{\Xi}_X = \mathbf{V}_{Q_X} \cdot / (1 + \mathbf{V}_{Q_X} \cdot \boldsymbol{\Gamma})$
- 4: $\gamma = (\epsilon + 1) \mathbf{1} \cdot / (L^{-1} (|\hat{\mathbf{X}}|^2 + \boldsymbol{\Xi}_X) \mathbf{1}_L)$
- 5: $\epsilon = \sqrt{\log(\langle \gamma \rangle) - \langle \log(\gamma) \rangle}$
- 6: $\boldsymbol{\Gamma} = \gamma \mathbf{1}_L^T$
- 7: Execute Lines (13)-(21) of UAMP-MF in Algorithm 2 to obtain \mathbf{V}_{Q_A} and \mathbf{Q}_A
- 8: $\forall z$: Construct \mathbf{E}_z and $\boldsymbol{\xi}_z$ according to (63).
- 9: $\forall z$: $\mathbf{V}_{c_z} = \sigma \left(\mathbf{E}_z^H \mathbf{E}_z \right)^{-1}$
- 10: $\forall z$: $\hat{\mathbf{c}}_z = \sigma^{-1} \mathbf{V}_{c_z} \mathbf{E}_z^H \boldsymbol{\xi}_z$
- 11: $\forall z$: $[d_z^{t+1}, \theta_z^{t+1}]^T = \hat{\mathbf{c}}_z + [d_z^t, \theta_z^t]^T$
- 12: $\boldsymbol{\Xi}_A = \frac{1}{Z} \sum_z \mathbf{E}_z \mathbf{V}_{c_z} \mathbf{E}_z^H$
- 13: $\hat{\mathbf{A}} = [\mathbf{a}(d_1, \theta_1), \dots, \mathbf{a}(d_Z, \theta_Z)]$
- 14: Execute Lines (24)-(25) of UAMP-MF in Algorithm 2

Until terminated

Output $[d_k, \theta_k]$ and perform differential demodulation.

We note that the number of candidate columns in $\hat{\mathbf{A}}$ can be often larger than K , i.e., its size is $R \times Z$, and the corresponding matrix $\hat{\mathbf{X}}$ has a size of $Z \times L$. Regarding this, we note the following.

- It is crucial to imposing a sparse prior on \mathbf{X} , so that the columns of $\hat{\mathbf{A}}$ with false distance-angle pairs correspond to a (nearly) zero row of $\hat{\mathbf{X}}$. In this paper, we adopt the Gauss-Gamma prior.
- We further note that the rows of $\hat{\mathbf{X}}$ have common support, which should be exploited to achieve better performance. This can be achieved using the Gauss-Gamma priors, where we impose that the elements of a row share a single precision γ_z . Hence, we have

$$\begin{aligned} p(\mathbf{X}) &= \prod_l p(\mathbf{x}_l | \gamma) p(\gamma) = \prod_{l,z} p(x_{z,l} | \gamma_z) p(\gamma_z) \\ &= \prod_{l,z} \mathcal{CN}(x_{z,l}; 0, \gamma_z^{-1}) \mathcal{G}(\gamma_z; \epsilon, \eta). \end{aligned} \quad (71)$$

- It is shown in [37] that, the performance of sparse signal recover can be significantly improved by automatically tuning the hyper parameter ϵ . We adopt the update rule in [37], i.e., ϵ is updated with the following equation in each iteration

$$\epsilon = \sqrt{\log(\langle \gamma \rangle) - \langle \log(\gamma) \rangle}, \quad (72)$$

where

$$\gamma = (\epsilon + 1) \mathbf{1}_L / \left(L^{-1} (|\hat{\mathbf{X}}|^2 + \Xi_X) \mathbf{1}_L \right). \quad (73)$$

The UAMP-MF based JNFLSD algorithm is summarized in Algorithm 3. The algorithm is an iterative one, and the iteration can be terminated when the difference between the estimates of \mathbf{A} or \mathbf{X} in two consecutive iterations is less than a threshold. At the end of the iteration, the algorithm outputs distance-angle pairs and the estimate $\hat{\mathbf{X}}$, based on which differential demodulation can be performed to make decision on the transmitted symbols. Regarding the algorithm, we have the following remarks.

- For the initialization of matrix \mathbf{A} , we propose to use a spatial power spectrum method, where the spatial power spectrum is defined as

$$\mathcal{S}(d_z, \theta_z) = \mathbf{a}(d_z, \theta_z)^H \mathbf{Y} \mathbf{Y}^H \mathbf{a}(d_z, \theta_z). \quad (74)$$

Through a coarse scan with the power spectrum, we can determine the areas where users may be located. Then these areas are divided uniformly with the distance-angle pairs $\{d_z, \theta_z\}$, based on which matrix \mathbf{A} can be initialized.

- The estimates of the matrices \mathbf{A} and \mathbf{X} are updated in each iteration. The rows of \mathbf{X} with small values and the corresponding columns of \mathbf{A} are killed, leading to low complexity of the iterative process.
- Thanks to the simultaneous estimation of \mathbf{A} and \mathbf{X} , the algorithm does not require the users to sent pilot signals, which makes the transmission efficient and suitable to dealing with dynamic scenarios. It is noted that, in the case that few pilot symbols are available, differential modulation is not needed.

V. SIMULATION RESULTS

Various simulation results are provided to verify the performance of the proposed UAMP-MF based JNFLSD algorithm. The system settings are as follows. A uniform linear antenna array with $R = 128$ elements and half-wavelength spacing is employed, and the center frequency $f_c = 30\text{GHz}$, so the Rayleigh distance is about 82 meters. We assume that K active users are uniformly distributed in an area of interest with distance range $[5\text{m}, d_{max}]$ and angle range $[30^\circ, 150^\circ]$. In the simulations, we vary the maximum distance d_{max} from 20m to 70m to investigate the impact of maximum distance on the performance of localization and communications. We compare the proposed UAMP-MF based JNFLSD algorithm with existing algorithms, including the on-grid SW-OMP algorithm [38], where far-field is assumed, the off-grid SIGW-OLS algorithm [15], where far-field is also assumed, and the on-grid algorithm NF-SOMP [9], [39], where near-field is assumed. The signal to noise power ratio (SNR) is defined as

$$\text{SNR} = \frac{\|\mathbf{A}\mathbf{X}\|^2 / RKL}{\sigma^2}, \quad (75)$$

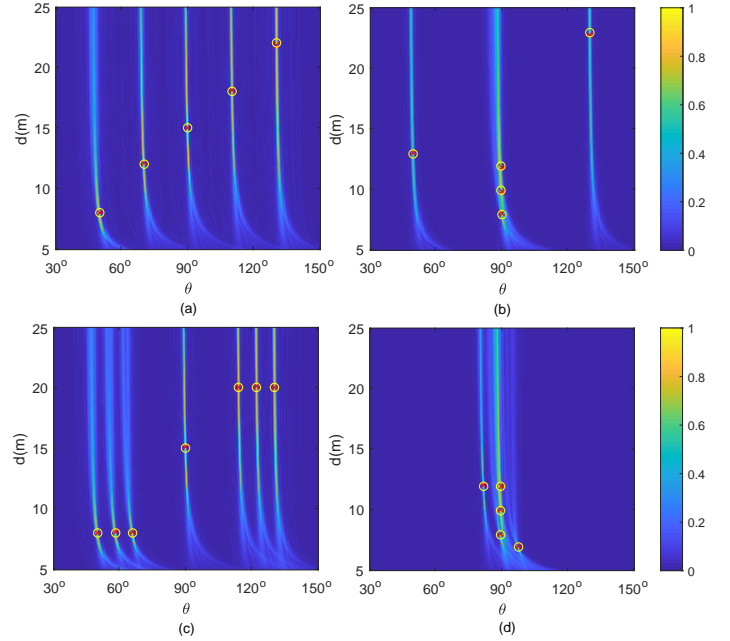


Fig. 4: Spatial power spectrum (normalized), the true locations (denoted by “o”) and estimated locations (denoted by “x”) of active users using the proposed algorithm.

where the numerator is the power of the received signal per antenna per user, and σ^2 is the power of noise. The localization performance is evaluated using the normalized mean squared errors (NMSE) of the distance estimation and the MSE of the angle estimation. The communication performance is evaluated using the bit error rate (BER) and frame error rate (FER).

We first examine the spatial power spectrum defined in (74) in Fig. 4 for some typical scenarios, where the spectrum is normalized and $\text{SNR} = -4\text{dB}$. The horizontal axis and vertical axis represent the angle and distance, respectively. We assume that there are 5 or 7 active users located within the area of interest, which are indicated using “o” in the figure. The estimated locations using the proposed UAMP-MF based algorithm are also shown, which are denoted by “x” in the figure. In Fig. 4(a), the users are well separated in both the angle domain and distance domain, which can be distinguished based on the spatial power spectrum. As expected, the UAMP-MF based algorithm can accurately localize all users. In Fig. 4(b), three users out of five users locate closely in the distance domain and angle domain, which can be hardly distinguished based on the spatial power spectrum. We can see that the UAMP-MF based algorithm can still estimate their locations accurately. In Fig. 4(c), there are 7 active users, where two groups of 3 users have the same distances with BS, and locate closely in the angle domain. Again the UAMP-MF based algorithm works well. Fig. 4(d) shows a challenging case, where all users locate closely in both angle and distance, where we can see that the proposed algorithm still delivers promising performance.

Next we compare the UAMP-MF based JNFLSD algorithm with SW-OMP, SIGW-OLS and NF-SOMP. It is noted that SW-OMP, SIGW-OLS and NF-SOMP all use a grid, and the grid size impacts their performance. In contrast, the proposed UAMP-MF based algorithm does not rely on the use of a grid. In addition, SW-OMP and SIGW-OLS assume far-field signal models and do

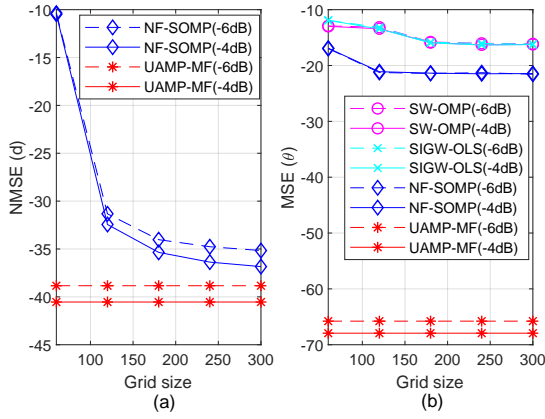


Fig. 5: (a) NMSE of distance estimation and (b) MSE of angle estimation versus grid size with $d_{max}=20\text{m}$ and $\text{SNR}=-4\text{dB}$ and -6dB .

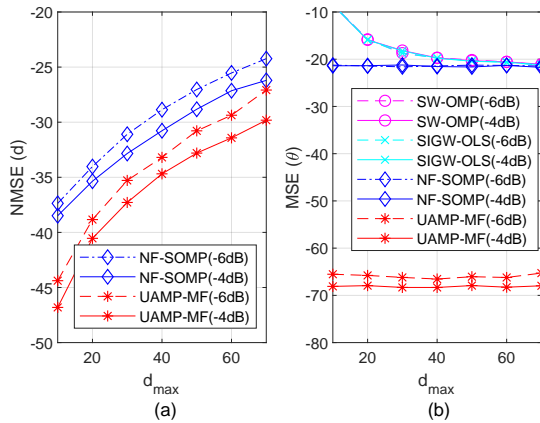


Fig. 6: (a) NMSE of distance estimation and (b) MSE of angle estimation versus d_{max} with $\text{SNR}=-4$ and -6dB .

not have the capability of distance estimation. So in evaluating the NMSE performance of distance estimation, SW-OMP and SIGW-OLS are absent. We first investigate the impact of grid size on the performance of the algorithms, and the NMSE of distance estimation and MSE of angle estimation are shown in Figs. 5 (a) and 5 (b), respectively. In the figures, the horizontal axis represents the number of grid points in angle (for SW-OMP, SIGW-OLS and NF-SOMF) and distance (for NF-SOMF). It can be seen that with the increase of grid points, the performance of SW-OMP, SIGW-OLS and NF-SOMF is improved but with the cost of increased complexity. When the number of grid points is larger than 240, the performance has no significant change. So, in subsequent simulations, for SW-OMP, SIGW-OLS and NF-SOMF, the number of grid points in angle and distance is set to 240, i.e., the grid size is 240×240 . From the results, we can see that the proposed algorithm significantly outperforms other algorithms in both distance estimation and angle estimation. In angle estimation, the performance of SW-OMP and SIGW-OLS is not good due to the model mismatch problem as they use the far-field assumption.

Then, we investigate the performance of localization versus the maximum distance d_{max} and the results are shown in Fig. 6. We can see that, the proposed algorithm achieves the best performance in all cases. With the increase of the maximum

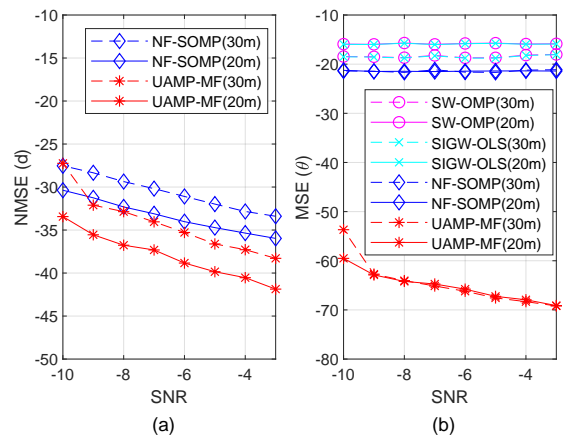


Fig. 7: (a) NMSE of distance estimation and (b) MSE of angle estimation versus SNR with $d_{max} = 20\text{m}$ and 30m .

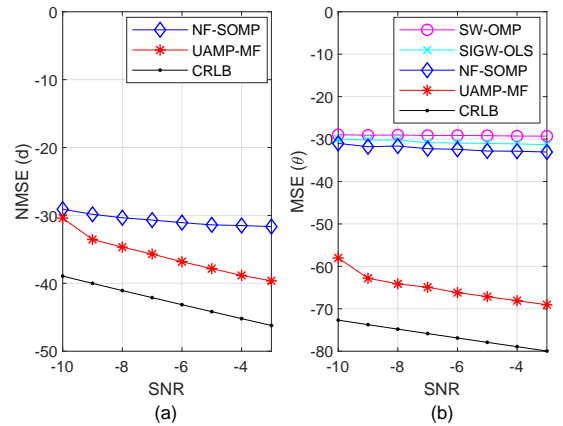


Fig. 8: Comparison with CRLB (a) distance estimation and (b) angle estimation.

distance d_{max} , the performance of distance estimation degrades, which is expected as the signal model tends to be a far-field one, where the contribution of the distance to the distance-angle steering vector diminishes. In contrast, the performance of the angle estimation does not change much with d_{max} , which is because in both near-field and far-field, the parameter of angle always plays an important role in the steering vector. It can also be observed from the figure that the performance of angle estimation of SW-OMP and SIG-OLS is improved considerably with the increase of distance. This is because, with the increase of the distance, the model mismatch due to the far-field assumption is alleviated. When the distance is small, the SW-OMP and SIG-OLS suffer from significant performance loss due to the severe model mismatch.

In Fig. 7, we show the NMSE of the distance estimation and MSE of angle estimation versus SNR, where the maximum distance $d_{max} = 20$ and 30 meters. As expected, with the increase of the SNR, the performance of distance estimation becomes better, and the proposed algorithm outperforms NF-SOMP consistently. We can see from 7 (b) that the MSE of angle estimation of the proposed algorithm is significantly better than that of other algorithms. In addition, the NMSE performance of angle estimation does not depend too much on the maximum distance d_{max} , which is consistent with the results in Fig. 6. In

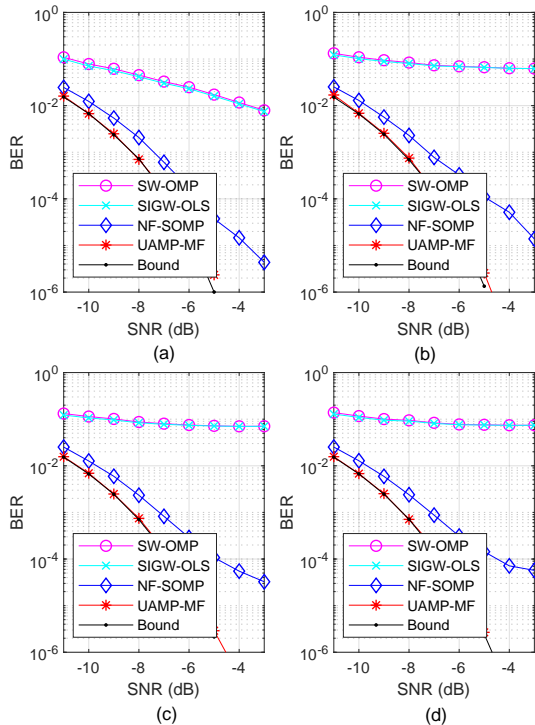


Fig. 9: BER versus SNR with $K = 1, 3, 5, 7$ and $d_{max}=30\text{m}$.

addition, the MSE of angle estimation of other algorithms does not improve too much with the SNR, which is because the grid mismatch or model mismatch dominate the errors.

We compare the performance of the algorithms with the CRLB, which is given in [5], and the results are shown in Fig. 8. In the simulations, we assume three users located at $(5.3\text{m}, 60.3^\circ)$, $(10.3\text{m}, 90.3^\circ)$ and $(15.3\text{m}, 120.3^\circ)$, respectively. We can see that, compared to other algorithms NF-SOMP, SW-OMP and SIGW-OLS, the proposed algorithm delivers performance much closer to the CRLB.

We compare the BER performance of the proposed algorithm with SW-OMP, SIGW-OLS and NF-SOMP. The results are shown in Fig. 9, where the number of users $K = 1, 3, 5, 7$ in (a), (b), (c) and (d), respectively. The FER performance is shown in Figs. 10 (a) and 10(b), where the number of users $K = 1$ and 3, respectively. In all cases, the maximum distance $d_{max}=30\text{m}$. In addition, we also show the BER and FER performance bounds, which are obtained by assuming the locations of all users are exactly known, i.e., the matrix \mathbf{A} is known. From the results we can see that, in all cases, SW-OMP and SIGW-OLS delivers poor BER performance. This is because they make far-field assumption, leading to significant model mismatch. We can also see that NF-SOMP only delivers good performance in the case of $K = 1$, and its performance deteriorates with the increase of K . This is because NF-SOMP adopts grid-based near-field model, and it works well in the case $K = 1$, where there is no inter-user interference. However, in the case of multiple users, NF-SOMP has limited capability to deal with the inter-user interference due to the energy leakage in determine the locations of the users, which results in a worse estimate of \mathbf{A} , thereby a worse estimate of \mathbf{X} . In all cases, the proposed algorithm delivers significantly better BER and FER performance, which is very close to the bounds.

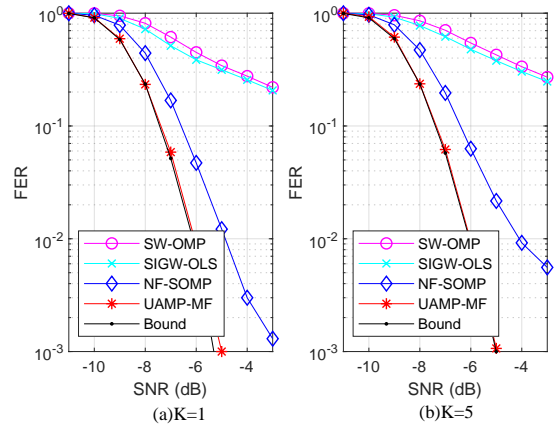


Fig. 10: FER versus SNR with $K = 1$ and 3 and $d_{max}=30\text{m}$.

VI. CONCLUSIONS

In this paper, we tackled the blind joint near-field localization and signal detection problem in an ISAC system, which is formulated as a MF problem with proper structures imposed on the factor matrices. By incorporating UAMP into variational inference through a whitening process, we designed the message passing algorithm UAMP-MF to solve a generic MF problem. Then, we apply the UAMP-MF algorithm to solve the joint localization and signal detection problem, where the factor matrix structures are fully exploited. Extensive simulation results demonstrate that the proposed algorithm significantly outperforms existing algorithms.

APPENDIX A PROOF OF PROPOSITION 1

According to VI, the message from f_Y to \mathbf{X} can be expressed as

$$\begin{aligned}
 & m_{f_Y \rightarrow \mathbf{X}}(\mathbf{X}) \\
 & \propto \exp \left(\int_{\mathbf{A}, \lambda} q(\mathbf{A}) q(\lambda) \log f_Y \right) \\
 & \propto \exp \left(-\hat{\lambda} \int_{\mathbf{A}} \text{Tr} \left((\mathbf{Y} - \mathbf{A}\mathbf{X})^H (\mathbf{Y} - \mathbf{A}\mathbf{X}) \right) q(\mathbf{A}) \right) \\
 & \propto \exp \left(-\hat{\lambda} \int_{\mathbf{A}} (\mathbf{y} - \text{Vec}(\mathbf{A}\mathbf{X}))^H (\mathbf{y} - \text{Vec}(\mathbf{A}\mathbf{X})) q(\mathbf{A}) \right) \\
 & = \exp \left(-\hat{\lambda} \int_{\mathbf{a}} (\mathbf{y} - \tilde{\mathbf{X}}\mathbf{a})^H (\mathbf{y} - \tilde{\mathbf{X}}\mathbf{a}) q(\mathbf{a}) \right) \quad (76) \\
 & = \exp \left(-\hat{\lambda} \int_{\mathbf{a}} (\mathbf{y}^H \mathbf{y} + \underbrace{\mathbf{a}^H \tilde{\mathbf{X}}^H \tilde{\mathbf{X}} \mathbf{a}}_{(i)} - \underbrace{\mathbf{a}^H \tilde{\mathbf{X}}^H \mathbf{y}}_{(ii)} - \underbrace{\mathbf{y}^H \tilde{\mathbf{X}} \mathbf{a}}_{(iii)}) q(\mathbf{a}) \right), \quad (77)
 \end{aligned}$$

where $\mathbf{a} = \text{Vec}(\mathbf{A})$, $\mathbf{y} = \text{Vec}(\mathbf{Y})$ and $\tilde{\mathbf{X}} = \mathbf{X}^H \otimes \mathbf{I}_M$. In the derivation of (76), we use the matrix identity $\text{Vec}(\mathbf{A}\mathbf{X}) = \text{Vec}(\mathbf{I}_M \mathbf{A}\mathbf{X}) = (\mathbf{X}^H \otimes \mathbf{I}_M) \mathbf{a}$ [40]. Next, we work out the integration of the three terms (i), (ii) and (iii) in (77). For

term (i), we have

$$\begin{aligned} & \int_{\mathbf{a}} \mathbf{a}^H \tilde{\mathbf{X}}^H \tilde{\mathbf{X}} \mathbf{a} q(\mathbf{a}) \\ &= \int_{\mathbf{a}} \text{Tr} \left(\tilde{\mathbf{X}}^H \tilde{\mathbf{X}} \mathbf{a} \mathbf{a}^H \right) q(\mathbf{a}) \\ &= \text{Tr} \left(\tilde{\mathbf{X}}^H \tilde{\mathbf{X}} (\hat{\mathbf{a}} \hat{\mathbf{a}}^H + \mathbf{V}_A \otimes \mathbf{U}_A) \right) \\ &= \text{Tr}(\hat{\mathbf{a}}^H \tilde{\mathbf{X}}^H \tilde{\mathbf{X}} \hat{\mathbf{a}}) + \text{Tr}(\tilde{\mathbf{X}} (\mathbf{V}_A \otimes \mathbf{U}_A) \tilde{\mathbf{X}}^H) \\ &= \text{Tr}(\text{Vec}(\hat{\mathbf{A}})^H (\mathbf{X}^H \otimes \mathbf{I}_M)^H (\mathbf{X}^H \otimes \mathbf{I}_M) \text{Vec}(\hat{\mathbf{A}})) \\ &\quad + \text{Tr}((\mathbf{X}^H \otimes \mathbf{I}_M) (\mathbf{V}_A \otimes \mathbf{U}_A) (\mathbf{X}^H \otimes \mathbf{I}_M)) \quad (78) \end{aligned}$$

$$\begin{aligned} &= \text{Tr}(\text{Vec}(\hat{\mathbf{A}} \mathbf{X})^H \text{Vec}(\hat{\mathbf{A}} \mathbf{X})) \\ &\quad + \text{Tr}((\mathbf{X} \otimes \mathbf{I}_M) (\mathbf{X}^H \otimes \mathbf{I}_M) (\mathbf{V}_A \otimes \mathbf{U}_A)) \quad (80) \end{aligned}$$

$$\begin{aligned} &= \text{Tr}(\mathbf{X}^H \hat{\mathbf{A}}^H \hat{\mathbf{A}} \mathbf{X}) \\ &\quad + \text{Tr}(((\mathbf{X} \mathbf{X}^H) \otimes \mathbf{I}_M) (\mathbf{V}_A \otimes \mathbf{U}_A)) \quad (81) \end{aligned}$$

$$= \text{Tr}(\mathbf{X}^H \hat{\mathbf{A}}^H \hat{\mathbf{A}} \mathbf{X}) + \text{Tr}(\mathbf{U}_A) \text{Tr}(\mathbf{X} \mathbf{X}^H \mathbf{V}_A) \quad (82)$$

$$= \text{Tr}(\mathbf{X}^H (\hat{\mathbf{A}}^H \hat{\mathbf{A}} + \text{Tr}(\mathbf{U}_A) \mathbf{V}_A) \mathbf{X}), \quad (83)$$

where we use the matrix identity $\text{Tr}(\mathbf{ABC}) = \text{Tr}(\mathbf{CAB})$ in deriving (80), $(\mathbf{A} \otimes \mathbf{B})(\mathbf{C} \otimes \mathbf{D}) = (\mathbf{AB}) \otimes (\mathbf{CD})$ and $(\mathbf{A} \otimes \mathbf{B})^H = \mathbf{A}^H \otimes \mathbf{B}^H$ in deriving (81), and $\text{Tr}(\mathbf{A} \otimes \mathbf{B}) = \text{Tr}(\mathbf{A})\text{Tr}(\mathbf{B})$ in deriving (82).

Regarding term (ii), we have

$$\begin{aligned} & \int_{\mathbf{a}} \mathbf{a}^H \tilde{\mathbf{X}}^H \mathbf{y} q(\mathbf{a}) \\ &= \int_{\mathbf{A}} \text{Vec}(\mathbf{A})^H (\mathbf{X}^H \otimes \mathbf{I}_M)^H \text{Vec}(\mathbf{Y}) q(\mathbf{A}) \\ &= \int_{\mathbf{A}} \text{Tr}(\mathbf{X}^H \mathbf{A}^H \mathbf{Y}) q(\mathbf{A}) \\ &= \text{Tr}(\mathbf{X}^H \hat{\mathbf{A}}^H \mathbf{Y}). \quad (84) \end{aligned}$$

Similarly, term (iii) can be expressed as

$$\int_{\mathbf{a}} \mathbf{y}^H \tilde{\mathbf{X}} \mathbf{a} q(\mathbf{a}) = \text{Tr}(\mathbf{Y}^H \hat{\mathbf{A}} \mathbf{X}). \quad (85)$$

Based on the above results, the message

$$\begin{aligned} m_{f_Y \rightarrow \mathbf{X}}(\mathbf{X}) &\propto \exp \left(-\hat{\lambda} \text{Tr}(\mathbf{X}^H (\hat{\mathbf{A}}^H \hat{\mathbf{A}} + \text{Tr}(\mathbf{U}_A) \mathbf{V}_A) \mathbf{X} \right. \\ &\quad \left. - \mathbf{X}^H \hat{\mathbf{A}}^H \mathbf{Y} - \mathbf{Y}^H \hat{\mathbf{A}} \mathbf{X} + \mathbf{Y}^H \mathbf{Y}) \right). \quad (86) \end{aligned}$$

Comparing the result against the matrix Gaussian distribution, we have the result shown in (17).

APPENDIX B PROOF OF PROPOSITION 2

According to VI, the message $m_{f_Y \rightarrow H}(\mathbf{A})$ is computed as

$$\begin{aligned} & m_{f_Y \rightarrow H}(\mathbf{A}) \\ &\propto \exp \left(\int_{\mathbf{X}, \lambda} q(\mathbf{X}) q(\lambda) \log f_Y \right) \\ &\propto \exp \left(-\hat{\lambda} \int_{\mathbf{X}} \text{Tr}((\mathbf{Y} - \mathbf{AX})^H (\mathbf{Y} - \mathbf{AX})) b(\mathbf{X}) \right) \\ &= \exp \left(-\hat{\lambda} \int_{\mathbf{x}} (\mathbf{y} - \tilde{\mathbf{A}} \mathbf{x})^H (\mathbf{y} - \tilde{\mathbf{A}} \mathbf{x}) b(\mathbf{x}) \right) \\ &= \exp \left(-\hat{\lambda} \int_{\mathbf{x}} (\mathbf{y}^H \mathbf{y} + \mathbf{x}^H \tilde{\mathbf{A}}^H \tilde{\mathbf{A}} \mathbf{x} \right. \\ &\quad \left. - \mathbf{x}^H \tilde{\mathbf{A}}^H \mathbf{y} - \mathbf{y}^H \tilde{\mathbf{A}} \mathbf{x}) b(\mathbf{x}) \right), \quad (87) \end{aligned}$$

where $\tilde{\mathbf{A}} \triangleq \mathbf{I}_L \otimes \mathbf{A}$. Similar to the derivation of (83), the integration of the terms in (87) can be expressed as

$$\int_{\mathbf{x}} \mathbf{x}^H \tilde{\mathbf{A}}^H \mathbf{y} b(\mathbf{x}) = \text{Tr}(\hat{\mathbf{X}}^H \mathbf{A}^H \mathbf{Y}) \quad (88)$$

and

$$\begin{aligned} & \int_{\mathbf{x}} \mathbf{x}^H \tilde{\mathbf{A}}^H \tilde{\mathbf{A}} \mathbf{x} b(\mathbf{x}) \\ &= \int_{\mathbf{x}} \text{Tr} \left(\tilde{\mathbf{A}}^H \tilde{\mathbf{A}} \mathbf{x} \mathbf{x}^H \right) b(\mathbf{x}) \\ &= \text{Tr}(\tilde{\mathbf{A}}^H \tilde{\mathbf{A}} (\hat{\mathbf{x}} \hat{\mathbf{x}}^H + \mathbf{V}_X \otimes \mathbf{U}_X)) \\ &= \text{Tr}(\hat{\mathbf{X}}^H \mathbf{A}^H \mathbf{A} \hat{\mathbf{X}}) + \text{Tr}(\mathbf{V}_X \otimes (\mathbf{A}^H \mathbf{A} \mathbf{U}_X)) \\ &= \text{Tr}(\hat{\mathbf{X}}^H \mathbf{A}^H \mathbf{A} \hat{\mathbf{X}}) + \text{Tr}(\mathbf{V}_X) \text{Tr}(\mathbf{A} \mathbf{U}_X \mathbf{A}^H) \\ &= \text{Tr}(\mathbf{A} (\hat{\mathbf{X}} \hat{\mathbf{X}}^H + \text{Tr}(\mathbf{V}_X) \mathbf{U}_X) \mathbf{A}^H). \quad (89) \end{aligned}$$

The message from f_Y to \mathbf{A} can be represented as

$$\begin{aligned} & m_{f_Y \rightarrow H}(\mathbf{A}) \\ &\propto \exp \left(-\hat{\lambda} \text{Tr}(\mathbf{Y} \mathbf{Y}^H + \mathbf{A} (\hat{\mathbf{X}} \hat{\mathbf{X}}^H + \text{Tr}(\mathbf{V}_X) \mathbf{U}_X) \mathbf{A}^H \right. \\ &\quad \left. - \mathbf{A} \hat{\mathbf{X}} \mathbf{Y}^H - \mathbf{Y} \hat{\mathbf{X}}^H \mathbf{A}^H \right). \quad (90) \end{aligned}$$

Comparing the above against the matrix Gaussian distribution, we obtain the result shown by (32) - (34).

APPENDIX C PROOF OF PROPOSITION 3

According to VI, the message

$$\begin{aligned} & m_{f_Y \rightarrow \lambda}(\lambda) \\ &= \det(\lambda^{-1} \mathbf{I}_M \otimes \mathbf{I}_L) \exp \left(-\lambda (\text{Vec}(\mathbf{Y}) - \text{Vec}(\mathbf{AX}))^H \right. \\ &\quad \left. (\text{Vec}(\mathbf{Y}) - \text{Vec}(\mathbf{AX})) \right) \\ &= \lambda^{ML} \exp \left(-\lambda \int_{\mathbf{A}, \mathbf{X}} \text{Tr}((\mathbf{Y} - \mathbf{AX})^H \right. \\ &\quad \left. (\mathbf{Y} - \mathbf{AX})) b(\mathbf{A}) b(\mathbf{X}) \right) \\ &= \lambda^{ML} \exp \left(-\lambda C \right), \quad (91) \end{aligned}$$

where

$$\begin{aligned} & C = \int_{\mathbf{A}, \mathbf{X}} \text{Tr}((\mathbf{Y} - \mathbf{AX})^H (\mathbf{Y} - \mathbf{AX})) q(\mathbf{A}) q(\mathbf{X}) \\ &= \int_{\mathbf{x}, \mathbf{A}} (\mathbf{y}^H \mathbf{y} + \mathbf{x}^H \tilde{\mathbf{A}}^H \tilde{\mathbf{A}} \mathbf{x} - \mathbf{x}^H \tilde{\mathbf{A}}^H \mathbf{y} - \mathbf{y}^H \tilde{\mathbf{A}} \mathbf{x}) q(\mathbf{x}) q(\mathbf{A}) \\ &= \int_{\mathbf{A}} \text{Tr}(\mathbf{Y} \mathbf{Y}^H + \mathbf{A} (\hat{\mathbf{X}} \hat{\mathbf{X}}^H + \text{Tr}(\mathbf{V}_X) \mathbf{U}_X) \mathbf{A}^H \\ &\quad - \mathbf{A} \hat{\mathbf{X}} \mathbf{Y}^H - \mathbf{Y} \hat{\mathbf{X}}^H \mathbf{A}^H) q(\mathbf{A}) \\ &= \text{Tr}(\mathbf{Y} \mathbf{Y}^H - \hat{\mathbf{A}} \hat{\mathbf{X}} \mathbf{Y}^H - \mathbf{Y} \hat{\mathbf{X}}^H \hat{\mathbf{A}}^H) \\ &\quad + \text{Tr}((\hat{\mathbf{X}} \hat{\mathbf{X}}^H + \text{Tr}(\mathbf{V}_X) \mathbf{U}_X) (\hat{\mathbf{A}}^H \hat{\mathbf{A}} + \text{Tr}(\mathbf{U}_A) \mathbf{V}_A)^H) \\ &= \text{Tr}((\mathbf{Y} - \hat{\mathbf{A}} \hat{\mathbf{X}})^H (\mathbf{Y} - \hat{\mathbf{A}} \hat{\mathbf{X}})) + \text{Tr}(\hat{\mathbf{X}} \hat{\mathbf{X}}^H \text{Tr}(\mathbf{U}_A) \mathbf{V}_A \\ &\quad + \text{Tr}(\mathbf{V}_X) \mathbf{U}_X \hat{\mathbf{A}}^H \hat{\mathbf{A}} + \text{Tr}(\mathbf{V}_X) \mathbf{U}_X \text{Tr}(\mathbf{U}_A) \mathbf{V}_A). \quad (92) \end{aligned}$$

By simplifying the above result, we obtain (44).

REFERENCES

- [1] M. Cui, Z. Wu, Y. Lu, X. Wei, and L. Dai, "Near-field mimo communications for 6g: Fundamentals, challenges, potentials, and future directions," *IEEE Communications Magazine*, vol. 61, no. 1, pp. 40–46, 2023.
- [2] Y. Lu and L. Dai, "Near-field channel estimation in mixed LoS/NLoS environments for extremely large-scale MIMO systems," *IEEE Transactions on Communications*, vol. 71, no. 6, pp. 3694–3707, 2023.
- [3] H. Elayan, O. Amin, B. Shihada, R. M. Shubair, and M.-S. Alouini, "Terahertz band: The last piece of rf spectrum puzzle for communication systems," *IEEE Open Journal of the Communications Society*, vol. 1, pp. 1–32, 2020.
- [4] T. S. Rappaport, Y. Xing, O. Kanhere, S. Ju, A. Madanayake, S. Mandal, A. Alkhateeb, and G. C. Trichopoulos, "Wireless communications and applications above 100 ghz: Opportunities and challenges for 6g and beyond," *IEEE Access*, vol. 7, pp. 78 729–78 757, 2019.
- [5] E. Grosicki, K. Abed-Meraim, and Y. Hua, "A weighted linear prediction method for near-field source localization," *IEEE Transactions on Signal Processing*, vol. 53, no. 10, pp. 3651–3660, 2005.
- [6] K. T. Selvan and R. Janaswamy, "Fraunhofer and fresnel distances: Unified derivation for aperture antennas," *IEEE Antennas and Propagation Magazine*, vol. 59, no. 4, pp. 12–15, 2017.
- [7] Z. Zhou, X. Gao, J. Fang, and Z. Chen, "Spherical wave channel and analysis for large linear array in los conditions," in *2015 IEEE Globecom Workshops (GC Wkshps)*, 2015, pp. 1–6.
- [8] Y. Cui, F. Liu, X. Jing, and J. Mu, "Integrating sensing and communications for ubiquitous iot: Applications, trends, and challenges," *IEEE Network*, vol. 35, no. 5, pp. 158–167, 2021.
- [9] X. Wei and L. Dai, "Channel estimation for extremely large-scale massive mimo: Far-field, near-field, or hybrid-field?" *IEEE Communications Letters*, vol. 26, no. 1, pp. 177–181, 2022.
- [10] F. Liu, Y. Cui, C. Masouros, J. Xu, T. X. Han, Y. C. Eldar, and S. Buzzi, "Integrated sensing and communications: Toward dual-functional wireless networks for 6g and beyond," *IEEE Journal on Selected Areas in Communications*, vol. 40, no. 6, pp. 1728–1767, 2022.
- [11] X. Mu, Z. Wang, and Y. Liu, "Noma for integrating sensing and communications towards 6g: A multiple access perspective," *IEEE Wireless Communications*, pp. 1–8, 2023.
- [12] Z. Wang, X. Mu, and Y. Liu, "Near-field integrated sensing and communications," *IEEE Communications Letters*, vol. 27, no. 8, pp. 2048–2052, 2023.
- [13] B. Zhao, C. Ouyang, X. Zhang, and Y. Liu, "On the performance of near-field isac," *ArXiv*, vol. <https://arxiv.org/abs/2310.10917>, 2023.
- [14] Z. Gao, C. Hu, L. Dai, and Z. Wang, "Channel estimation for millimeter-wave massive mimo with hybrid precoding over frequency-selective fading channels," *IEEE Communications Letters*, vol. 20, no. 6, pp. 1259–1262, 2016.
- [15] N. González-Prelcic, H. Xie, J. Palacios, and T. Shimizu, "Wideband channel tracking and hybrid precoding for mmwave mimo systems," *IEEE Transactions on Wireless Communications*, vol. 20, no. 4, pp. 2161–2174, 2021.
- [16] Y. Han, S. Jin, C.-K. Wen, and X. Ma, "Channel estimation for extremely large-scale massive mimo systems," *IEEE Wireless Communications Letters*, vol. 9, no. 5, pp. 633–637, 2020.
- [17] W. Zuo, J. Xin, N. Zheng, and A. Sano, "Subspace-based localization of far-field and near-field signals without eigendecomposition," *IEEE Transactions on Signal Processing*, vol. 66, no. 17, pp. 4461–4476, 2018.
- [18] M. Cui and L. Dai, "Channel estimation for extremely large-scale mimo: Far-field or near-field?" *IEEE Transactions on Communications*, vol. 70, no. 4, pp. 2663–2677, 2022.
- [19] B. Friedlander, "Localization of signals in the near-field of an antenna array," *IEEE Transactions on Signal Processing*, vol. 67, no. 15, pp. 3885–3893, 2019.
- [20] J. Winn and C. M. Bishop, "Variational message passing," *J. Mach. Learn. Res.*, vol. 6, pp. 661–694, Apr. 2005.
- [21] Q. Guo and J. Xi, "Approximate message passing with unitary transformation," *arXiv preprint arXiv:1504.04799*, Apr. 2015.
- [22] Z. Yuan, Q. Guo, and M. Luo, "Approximate message passing with unitary transformation for robust bilinear recovery," *IEEE Trans. Signal Process.*, vol. 69, pp. 617–630, Dec. 2020.
- [23] D. J. De Waal, *Matrix-Valued Distributions*. Encyclopedia of Statistical Sciences, 1985.
- [24] T. S. Rappaport, Y. Xing, G. R. MacCartney, A. F. Molisch, E. Mellios, and J. Zhang, "Overview of millimeter wave communications for fifth-generation (5g) wireless networks—with a focus on propagation models," *IEEE Transactions on Antennas and Propagation*, vol. 65, no. 12, pp. 6213–6230, 2017.
- [25] R. Rubinstein, A. M. Bruckstein, and M. Elad, "Dictionaries for sparse representation modeling," *Proceedings of the IEEE*, vol. 98, no. 6, pp. 1045–1057, June 2010.
- [26] H. Zhu, G. Leus, and G. B. Giannakis, "Sparsity-cognizant total least-squares for perturbed compressive sampling," *IEEE Transactions on Signal Processing*, vol. 59, no. 5, pp. 2002–2016, May 2011.
- [27] E. J. Candes, X. Li, Y. Ma, and J. Wright, "Robust principal component analysis?" *J. ACM*, vol. 58, no. 3, Jun. 2011. [Online]. Available: <https://doi.org/10.1145/1970392.1970395>
- [28] J. T. Parker, P. Schniter, and V. Cevher, "Bilinear generalized approximate message passing, part i: Derivation," *IEEE Transactions on Signal Processing*, vol. 62, no. 22, pp. 5839–5853, 2014.
- [29] D. M. Blei, A. Kucukelbir, and J. D. McAuliffe, "Variational inference: A review for statisticians," *Journal of the American Statistical Association*, vol. 112, no. 518, pp. 859–877, apr 2017. [Online]. Available: <https://doi.org/10.1080/2F01621459.2017.1285773>
- [30] J. Dauwels, "On variational message passing on factor graphs," in *2007 IEEE International Symposium on Information Theory*, 2007, pp. 2546–2550.
- [31] D. L. Donoho, A. Maleki, and A. Montanari, "Message-passing algorithms for compressed sensing," *Proc. Nat. Acad. Sci.*, vol. 106, no. 45, pp. 18 914–18 919, Nov. 2009.
- [32] S. Rangan, "Generalized approximate message passing for estimation with random linear mixing," in *Proc. Int. Symp. Inf. Theory*. IEEE, July. 2011, pp. 2168–2172.
- [33] S. Rangan, P. Schniter, A. K. Fletcher, and S. Sarkar, "On the convergence of approximate message passing with arbitrary matrices," *IEEE Trans. Inf. Theory*, vol. 65, no. 9, pp. 5339–5351, Sept. 2019.
- [34] M. E. Tipping, "Sparse bayesian learning and the relevance vector machine," *J. Mach. Learn. Res.*, vol. 1, pp. 211–244, sep 2001. [Online]. Available: <https://doi.org/10.1162/15324430152748236>
- [35] H. Ishwaran and J. S. Rao, "Spike and slab variable selection: Frequentist and Bayesian strategies," *The Annals of Statistics*, vol. 33, no. 2, pp. 730 – 773, 2005. [Online]. Available: <https://doi.org/10.1214/009053604000001147>
- [36] C. M. Carvalho, N. G. Polson, and J. G. Scott, "Handling sparsity via the horseshoe," in *Proceedings of the Twelfth International Conference on Artificial Intelligence and Statistics*, 2009, pp. 73–80.
- [37] M. Luo, Q. Guo, M. Jin, Y. C. Eldar, D. Huang, and X. Meng, "Unitary approximate message passing for sparse bayesian learning," *IEEE Transactions on Signal Processing*, vol. 69, pp. 6023–6039, 2021.
- [38] J. Rodríguez-Fernández, N. González-Prelcic, K. Venugopal, and R. W. Heath, "Frequency-domain compressive channel estimation for frequency-selective hybrid millimeter wave mimo systems," *IEEE Transactions on Wireless Communications*, vol. 17, no. 5, pp. 2946–2960, 2018.
- [39] J. Tropp, A. Gilbert, and M. Strauss, "Simultaneous sparse approximation via greedy pursuit," in *Proceedings. (ICASSP '05). IEEE International Conference on Acoustics, Speech, and Signal Processing, 2005.*, vol. 5, 2005, pp. v/721–v/724 Vol. 5.
- [40] K. B. Petersen and M. S. Pedersen, *The Matrix Cookbook*. on-line, Sep. 2007, <http://matrixcookbook.com>.